Universidade Federal de Juiz de Fora

Engenharia Elétrica

Programa de Pós-Graduação em Engenharia Elétrica

Michelle Soares Pereira

**Cooperative In-home Power Line Communication: Analyses Based on a
Measurement Campaign**

Juiz de Fora

2015

Cooperative In-home Power Line Communication: Analyses Based on a Measurement Campaign

Dissertação de mestrado apresentada ao Programa de Pós-Graduação em Engenharia Elétrica da Universidade Federal de Juiz de Fora, na área de concentração em sistemas eletrônicos, como requisito parcial para obtenção do título de Mestre em Engenharia Elétrica.

Orientador: Moisés Vidal Ribeiro

Juiz de Fora

2015

Michelle Soares Pereira

Cooperative In-home Power Line Communication: Analyses Based on a Measurement Campaign

Dissertação de mestrado apresentada ao Programa de Pós-Graduação em Engenharia Elétrica da Universidade Federal de Juiz de Fora, na área de concentração em sistemas eletrônicos, como requisito parcial para obtenção do título de Mestre em Engenharia Elétrica.

Aprovada em:

BANCA EXAMINADORA

_____
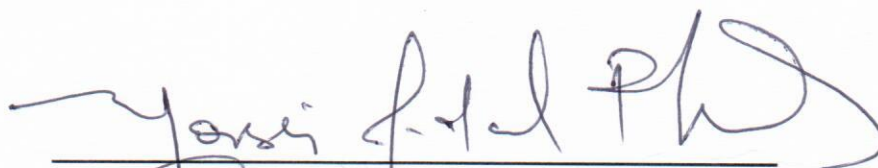
Moisés Vidal Ribeiro - Orientador
Universidade Federal de Juiz de Fora

_____

Professor Dr. Raimundo Sampaio Neto
Pontifícia Universidade Católica do Rio de Janeiro

_____
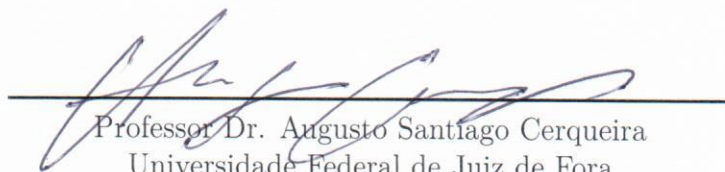
Professor Dr. Augusto Santiago Cerqueira
Universidade Federal de Juiz de Fora

Dedico este trabalho a minha mãe Sandra, meu pai Wellington, minha irmã Priscila e meu marido Alex.

AGRADECIMENTOS

"O sucesso requer assumir riscos, enfrentar seus medos, e acima de tudo, acreditar que é possivel."

(Autor desconhecido)

RESUMO

Este trabalho aborda a análise de protocolos de cooperação para melhorar o desempenho de sistemas *powerline communication* (PLC). O estudo se baseia em um conjunto de dados de canais PLC in-home. As análises discutidas abordam a capacidade teórica do canal quando protocolos *amplify-and-forward* (AF) e *decode-and-forward* (DF) são considerados. Estudos similares são realizados a respeito da taxa máxima de dados adquirida quando *Hermitian − symmetric orthogonal frequency division multiplexing* (HS-OFDM) juntamente com as técnicas *equal gain combining* (EGC), *selection combining* (SC) and *maximal ratio combining* (MRC) são considerados. Além disso, são analisadas as influências da largura de banda de freqüência e da alocação ótima e uniforme da potência de transmissão. Os resultados obtidos mostram que a distância relativa entre os nós da fonte, *relay* e destino impactam severamente no desempenho do sistema. Os resultados numéricos revelam uma gama de potência de transmissão ótima e de frequência em que a melhoria pode ser verificada. TambÃ©m observa-se que a vantagem do protocolo DF relacionada com a do protocolo AF termina quando o erro de detecção de símbolo no *relay* atinge um limiar. Adicionalmente, mostra-se que as técnicas de combinação, MRC e SC apresentam resultados semelhantes. Embora MRC ofereça desempenho ligeiramente melhor, considerando a complexidade computacional, recomenda-se a técnica SC. Finalmente, uma análise de máxima taxa de dados adquirida, considerando HS-OFDM com equalização baseada nos critérios *zero forcing* e *minimum mean square error*, mostra que o primeiro oferece quase o mesmo desempenho que o último.

Palavras-chave: Canal PLC in-home cooperativo, capacidade teórica do canal, máxima taxa de dados, protocolos AF e DF, técnicas de combinação.

ABSTRACT

This work focuses on analyses of cooperative protocols to enhance the performance of in-home power line communication (PLC) systems based on a data set consisting of measurements of in-home PLC channels. The discussed analyses address theoretical channel capacity when amplify-and-forward (AF) and decode-and-forward (DF) protocols are considered. Similar investigations are performed for the maximum data rate attained by using Hermitian-symmetric orthogonal frequency division multiplexing (HS-OFDM) together with equal gain combining (EGC), selection combining (SC) and maximal ratio combining (MRC) techniques. Also, the influences of optimally and uniformly allocated transmission power and frequency bandwidth are analyzed. The attained results show that the relative distance among source, relay, and destination nodes severely impacts the system performance. Also, numerical results reveal a range of optimal transmission power and frequency bandwidth in which improvement can be verified. Moreover, it is observed that the advantage of the DF protocol related to AF one ends, when the symbol detection error achieves a threshold. Additionally, it is shown that among the combining techniques, MRC and SC present similar results with MRC offering slightly better performance, but considering computational complexity, a decision in favor of SC is recommended. Finally, a maximum data rate analysis of HS-OFDM with frequency domain equalizer based on zero forcing and minimum mean square error shows that the former scheme offers almost the same performance as the latter.

Key-words: In-home cooperative and in-home PLC channel, theoretical channel capacity, maximum data rate, AF and DF protocols, combining techniques.

LIST OF FIGURES

LIST OF TABLES

ACRONYMS

AF amplify-and-forward

AM amplitude modulation

AWGN additive white Gaussian noise

CGRC circular Gaussian relay channel

CP cyclic prefix

CSI channel state information

DF decode-and-forward

DFT discrete Fourier transform

DSL digital subscriber line

EGC equal gain combining

FDE frequency domain equalization

FM frequency modulation

HS-OFDM hermitian symmetric orthogonal frequency division multiplexing

ICI inter carrier interference

ISI inter symbol interference

LTI linear time invariant

MIMO multiple-input multiple-output

MMSE minimum mean square error

MRC maximal ratio combining

OA optimal power allocation

OFDM orthogonal frequency division multiplexing

PLC power line communication

PSD power spectral density

SC selection combining

SC-CP single-carrier with cyclic prefix

SNR signal-to-noise ratio

UA uniform power allocation

ZF zero-forcing

CONTENTS

1 INTRODUCTION

Power line communication (PLC) is the technology that makes use of existing infrastructure of power systems to perform data communication. Recently, this technology has received considerable attention because of their low installation costs and ubiquitousness. On the other hand, as the electric power grids were not designed to this end, they are a challenging medium for data communication. For example, electric power cables are not shielded, being characterized by the presence of impulsive noise with high power. In addition to that, the channel is time-varying and the signal attenuation increases with frequency and distance. Also, there are regulatory rules that impose severe restrictions on the use of PLC technology to avoid interference in other communication service primary users operating in the same frequency band [1].

To improve PLC system performance under these constraints, several techniques have been investigated. Among them, it can be mentioned orthogonal frequency division multiplexing (OFDM), single-carrier with cyclic prefix (SC-CP), resource allocation, impulsive noise mitigation and powerful channel coding [5]. More recently, the investigation of cooperative communication has attracted more attention in order to introduce improvement in the performance of PLC systems.

The idea of cooperation is not new, it has been the focus of research for wireless networks, covering, among others, mobile, ad-hoc and wireless local area [6]. Thus, users can cooperate with each other in order to obtain mutual gains in environments where the data communication conditions are unfavorable. Cooperation among users does not only lead to higher data rates, but also increases the flexibility and reliability of data communication systems.

Due to the broadcast nature of channel, the power electric grids became a very attractive candidate to receive cooperative communication. Therefore, there is a growing effort to investigate the suitability of cooperative concepts for improving PLC systems on in-home electric power grids. Although the attained results appeal in favor of this technique, they are based on the use of theoretical models and computational simulations for the PLC channel corrupted by additive noises.

Although the attained results obtained with the theoretical models of PLC channels motivate more investigations of the benefits of cooperative communication for PLC systems, there is a lack of analyses based on measured data that could offer additional information to verify the suitability of cooperative communication for this challenging channel.

1.1 Objectives

In this context, this dissertation has the following main contributions:

- To a present comprehensive analyses in terms of theoretical channel capacity of cooperative communications on in-home PLC systems by using a data set composed of measured in-home PLC channels which was obtained from a measurement campaign addressing typical residences in a Brazilian city.

- To perform the maximum data rate analyses of hermitian symmetric orthogonal frequency division multiplexing (HS-OFDM) scheme [7] with frequency domain equalizer (FDE) based on zero-forcing (ZF) and maximum mean square error (MMSE) criteria, together with equal gain combining (EGC), selection combining (SC) and maximal ratio combining (MRC) techniques [6] for data communication through the cooperative and in-home PLC channels.

1.2 Dissertation Outline

This work is organized as follows: Chapter 2 reviews some concepts about cooperative in-home PLC channels; Chapter 3 presents the adopted assumptions related to the theoretical channel capacities and maximum data rates when HS-OFDM scheme with frequency domain equalization (FDE)-zero-forcing (ZF) and FDE-minimum mean square error (MMSE) are taken into account. Chapter 4 describes the measurement campaign. Chapter 5 presents numerical analyses of measured data. Finally, concluding remarks are given in Chapter 6.

1.3 Summary

This chapter presented a brief introduction of this dissertation. Also, the main objectives and the organization of this work were summarized.

2 LITERATURE REVIEW

A growing interest in the use of electric power grids for data communication purposes is notorious. Indeed, PLC systems and their applications have been widely investigated by academic and business sectors [1] . However, as electric power grids were not originally designed for communication purposes, they constitute a challenging data communication medium, in which the transmitted signals suffer severe attenuations and are strongly corrupted by colored and impulsive noise. The diversity of topologies of electric power grids and the dynamic operation of the connected loads make these grids hard to characterize and model.

A promising approach that has been studied to overcome these limitations is the use of cooperative communication concepts. This technique addresses cooperative protocols and strategies applied at the physical layer, offering benefits related to channel capacity and coverage to the PLC systems. Thereby, for a deep knowledge of this subject, it is critical to understand the behavior of PLC channels and tools utilized for their analysis.

To this end, this chapter is organized as follows: Section 2.1 discusses the communication channel via indoor electric power grids. A review of cooperative communication, exploring its origin and addressing the motivation of its use in PLC systems is presented in Section 2.2, while some concepts on HS-OFDM scheme are discussed in Section 2.3.

2.1 Indoor PLC Channels

The idea of data transmission over power line dates back to 1920, when the first proposals to use carriers to perform communication networks in high voltage were used. In the 80s, some electric utilities of United States and Europe began to analyze the main characteristics of this technology as a communication channel. The tests revealed that the frequencies between 5 and 500 kHz had the greatest potential, mainly due to the signal-to-noise ratio (SNR) and signal attenuation [8]

In 1991, some tests were initiated with high-speed communication in England. In 1997, it was announced by the Norweb and Nortel, two electric utilities in England, that the problems caused by noise and interference had been solved.

Since then, the data transmission over the electric power grids have been the subject of several studies in the data communication sector due to the feasibility of its implementation for smart grid communication and broadband access network applications.

PLC is a technology classified as without new wires because it is characterized by the use of the electric power grids as data transmission medium, which significantly reduces the costs related to implementation of a new infrastructure of communication. According to [3], the investments involved in the implementation and maintenance of
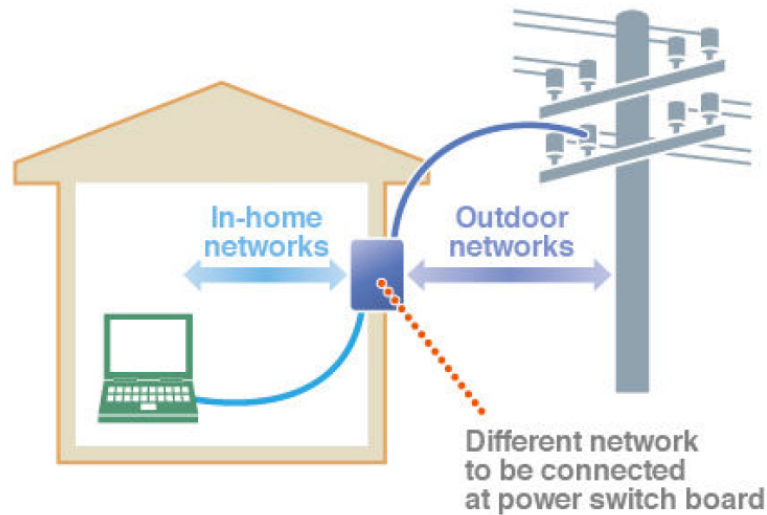
Figure 1: Structure PLC network.

access networks represent about 50% of the total cost and, therefore, the PLC technology has a strong economic viability in environments without communications infrastructure, but with electric power infrastructure. In addition, this technology also enables digital inclusion since about 98% of population in the world is served by the electric power service.

On the other hand, the electric power grids were designed to the power transmission considering low frequency (50 or 60 Hz) and high power. Therefore, the technical challenges for transmission data at high frequencies and low power are significant. Indeed, as the power cables are not ideal conductors, the signal attenuation increases as the frequency and distance increase, which impose limits on the use of PLC technology. Furthermore, the presence of time varying loads changes, over time, the behavior of the electric power grids. Usually, the following phenomena are observed: impedance mismatch, temporal variation of the channel impulse response, impulsive noise with high power, either synchronous or not with the main frequency. Furthermore, since power cables are unshielded, they interfere and suffer interference of other communications systems operating in the same frequency range, such as digital subscriber line (DSL), amateur radio, cable TV, amplitude modulation (AM) and frequency modulation (FM) stations.

According to the environment in which this technology is employed, the PLC systems can be classified as indoor and outdoor as indicated in Figure 1. While indoor refers to the use of electric low voltage circuit in buildings, residences and vehicles; the term outdoor refers to the underground/aerial transmission and distribution power system infrastructure. As the outdoor networks of medium and high voltage present few connections in relation to low voltage networks and, beyond that, the transformers operate as open circuits at high frequencies, the outdoor environment is characterized by less hostile conditions compared those in the indoor environment.

Concerning the technical challenges that this new technology must overcome on
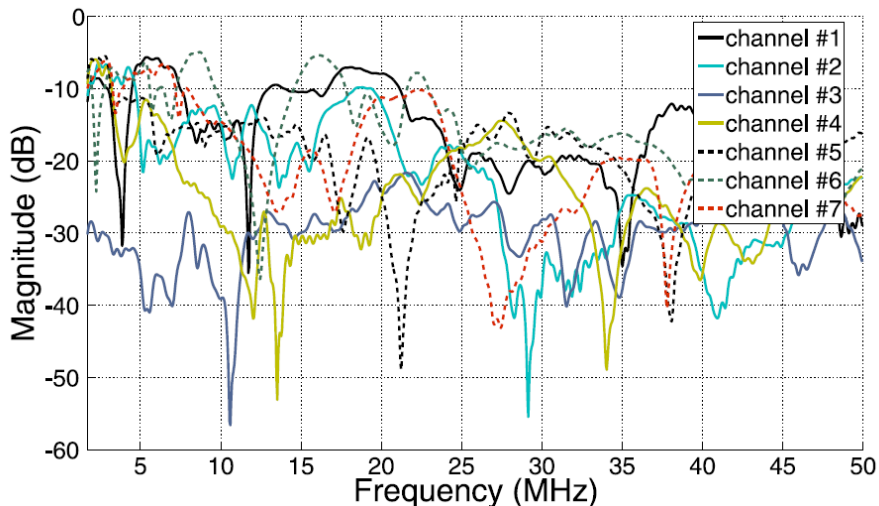
Figure 2: Magnitude of the frequency response of seven measured PLC channels [1].

indoor environments, the topology of electric power grids has several branches, favoring the signal reflections. Those echoes, also known by the multipath phenomenon, often occur due to impedance mismatches in the connection points among power cables and electrical equipment because the value of load impedance can vary over time, frequency, location and the connection among power cables deteriorates with time. Thereby, the resultant impulse response of the channel consists of several delayed echoes of the main impulse, which means a frequency response with deep notches of high attenuation. All these properties can be observed in Figure 2, where some channel responses are plotted.

A simplified and widely used model addresses a linear time invariant (LTI) PLC channel, when the load connected to the electric power grid does not change over time. This type of modeling can be considered when there is not impedance variation. To model this channel, two strategies are adopted; the first, *top-down*, sets the multi-propagation model for the channel behavior from measurement campaigns, characterizing it by the existence of a finite number of paths. Another strategy also adopted is the *bottom-up* in which, a priori, the channel parameters are defined from physical characteristics of the electric power grid and then, it is constituted the behavioral parametric model [9].

Unlike other data communication medium, the electric power grids are not characterized by the existence of an additive white Gaussian noise (AWGN), in which the power spectral density (PSD) is constant over the considered frequency spectrum. On further analysis, according to [8], the PLC noise is the composition of other three types of different noises classified according to its origin, duration time, occupation and PSD. They are:

- Background noise is the total sum of various noise sources with low power and its PSD is usually around -145 dBm/Hz;
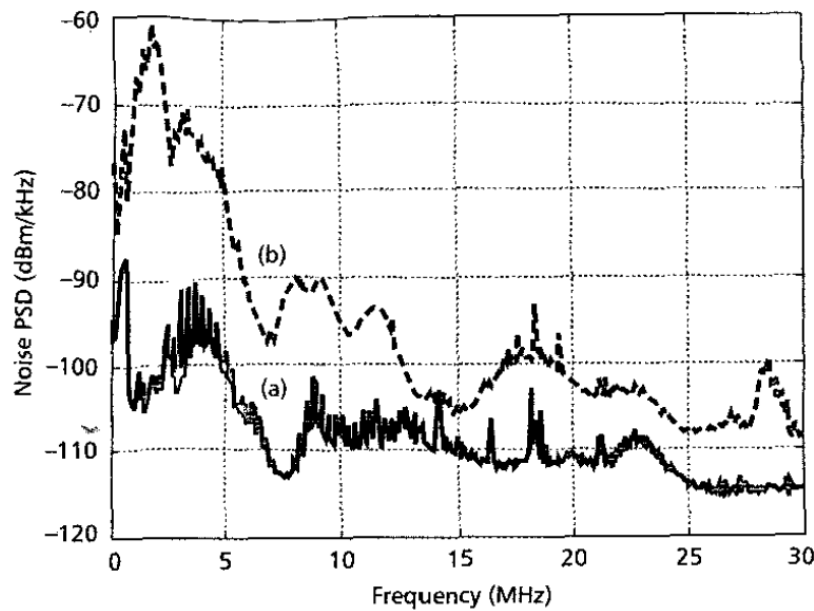
Figure 3: Measurements of indoor background noise PSD: a) in an apartment; b) in a university laboratory [2].

- Narrow band noise is caused by induction from radio station signals in medium and short waves bands;

- The impulsive noise is caused by transients due to switching phenomena within the electric power grids and it has maximum amplitude of 40 dBm/Hz higher than background and/or narrow band noise.

These three types of noise described above are arranged in two groups. The general background noise, whose PSD is shown in Figure 3, comprises less severe noisy distortions. This is considered as the superposition of colored noise and narrow band disturbances. On the other hand, the impulsive noise, represented by the Figure 4, is strongly dominated by the aperiodic noise which varies in a few period of time, and so, it is the main cause of transmission errors in PLC channels.

Currently, there is a reasonable understanding of the communication medium defined by indoor electric power grids. For example, [10] demonstrates the technical viability of PLC systems on medium and low-voltage grids from the continued operation for more than ten months in the United States. [11] mentions that although broadband PLC is an excellent home networking technology to complement the WiFi service and several industry alliances were formed with a charter to set technology specification mostly for in-home PLC, none of the technologies are inter operable with each other. This problem was later addressed with PLC standards [12, 13] and technologies [14–17] offering up to 1 Gbps at the physical layer.

The characterization of additive noise, access impedance and overall channel
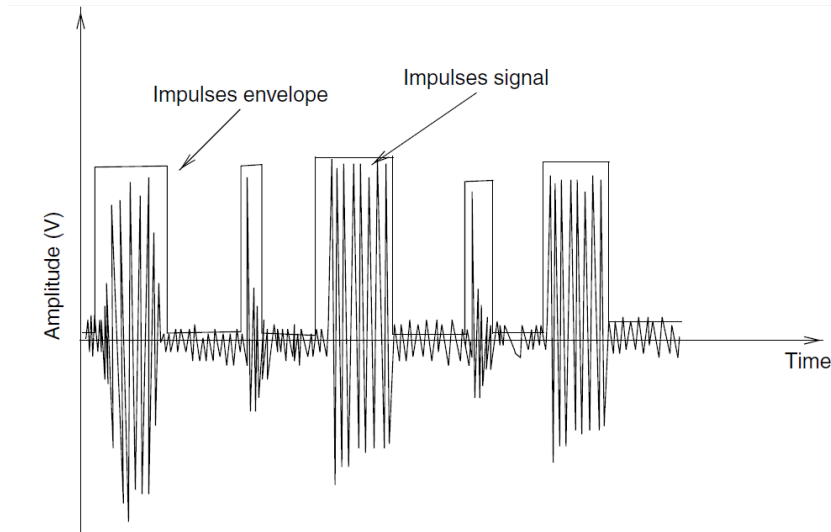
Figure 4: Example of impulsive noise in time domain [3].

behavior in the frequency bandwidth up to 300 MHz of these grids is being better reported in the literature. For example, while [18] proposes a channel parametric model for broadband indoor PLC based on the physical structure of the electric power grids inside homes and small offices, [19] models, deterministically and in the frequency domain, the PLC transfer function. Additionally, [1] is the first thesis of our research group that addresses a methodology applied to characterize indoor electric power grids for data communication purposes in underdeveloped countries. This methodology covers all the procedures and details of the signal processing tools for a reliable estimation of important features for the evaluation of communication channels.

A common aspect of all aforementioned contributions is that they agreed that the PLC channels are highly impaired and advances need to be introduced to improve the system performance.

2.2 Cooperation

The idea of cooperation is relatively recent and strongly related to wireless technology. The classical relay channel introduced by Van der Meulen in 1971 was constituted by three-terminal communication channel. Soon after, Cover and El Gamal developed in 1979 the lower and upper bounds on the channel capacity for specific non-faded relay channel models. Later, several works have studied the capacity of the relay channels and developed coding strategies that can achieve the ergodic channel capacity under certain scenarios. Laneman, around 2000, proposed different cooperative diversity protocols and analyzed their performance in terms of outage behavior [4].

The cooperative communications consists of independent paths generated via the introduction of a relay channel. The relay channel is an auxiliary path to the direct link
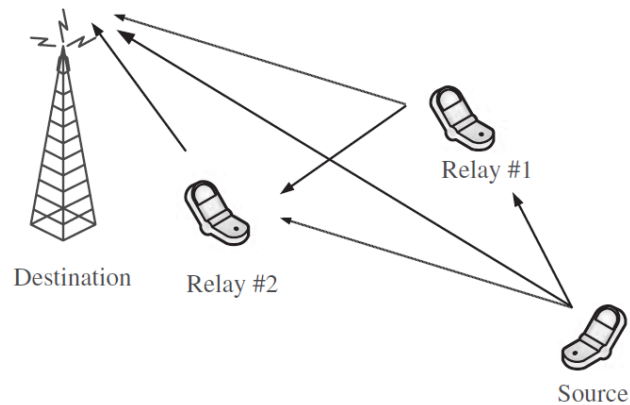
Figure 5: Example of wireless cooperative network [4].

between the source and destination, as the example shown in Figure 5 for a wireless network. The main aspect of the cooperative communication is the processing of the signal received at the relay node. Some different processing schemes result in different cooperative communication protocols.

Cooperative communications protocols can be categorized into several kinds, among them amplify-and-forward (AF) and decode-and-forward (DF) are the most basic and widely adopted. In the AF protocol, the relay simply amplifies the received version and transmits it to the destination node and so this protocol is classified as non regenerative. On the other hand, the DF protocol is regenerative because the relay decodes the received signal, re-encodes it and then retransmits it to the destination [6].

In this way, two copies from the transmitted signal by the source arrive at the receiver, one coming through the direct link and another coming through the cooperative link. To deal with these signals, there are four principal types of combining techniques depending essentially on the complexity restrictions put on the data communication system and amount of perfect channel state information (CSI) available, as it is listed below:

- In the EGC combining technique, the signals received are each one multiplied by a complex weighting factor that compensates the phase rotation of channel. It achieves phase coherence at the receiver and, thus, increases considerably the resultant signal strength. On the other hand, it is often difficult to implement in practice since the phase of channel varies rapidly over time. When the signal phases cannot be perfectly identified, the combination may result in a destructive interference;

- The MRC combining technique maximizes the overall SNR, so it requires a coherent detector. In the absence of interference, MRC is the optimal combining scheme. Since it requires knowledge of all channel fading parameters, this scheme demands some computational complexity.

- Unlike the EGC and MRC combining techniques that require some or all CSI (fading amplitude, phase, and delay) of the received signals, adding to the overall receiver complexity, the SC is the simplest technique. Specifically, it processes only one of the diversity branches because it chooses the branch with the highest SNR. In addition, since the output of the SC combiner is equal to the signal on only one of the branches, the coherent sum of the individual branch signals is not required;

Regarding the PLC technology, to deal with the limitations of channels, some additional tools have been investigated and among them is the cooperative communication. For example, [5] mentions that the spatial dimension of the PLC network becomes infeasible the direct communication between the central node and all other connected devices and, therefore, to achieve complete coverage, messages need to be repeated, which is also known as multi hop transmission or relaying. This way, such a repeater concept makes optimal use of the available communication nodes in the network and is flexible enough to also ensure network coverage and communication reliability under changing topologies and channel conditions.

In [20], a particular coding for multi hop transmission without the need for complex routing protocols was addressed. When no further signal processing is applied at the transmitter, simultaneous retransmissions often deteriorate the performance compared to the single-node retransmission. The work [21] considers the effect of self-interference generated by relay nodes and tries to suppress it. It is also shown that the multiple-input multiple-output (MIMO) architecture can strongly improve the PLC performance and reliability of links. According to it, the spatial multiplexing is a powerful tool to maximize the good-put network. An opportunistic cooperative system to provide power saving, quality of service, coverage and range extension is discussed in [22] and [23]. In this case, the relay only acts in certain situations when the channel capacity with the DF protocol is higher than that achievable through the direct link.

On the other hand, an investigation of cooperative channel coding for PLC system, covering narrow band application, was addressed in [24]. Considering such multihop PLC as a bus system, the authors demonstrate, in this work, the benefits in terms of achievable data rate derived from the application of cooperative coding. Moreover, the analysis of the AF protocol for improving PLC system in medium-voltage electric power grids was discussed in [25] where it was shown that the channel capacity of the proposed protocol increases as the number of relay nodes increases.

Furthermore, a theoretical channel capacity analysis of the improvement offered by the AF protocol was presented in [26] and numerical results showed that, through the optimal power allocation, this protocol can provide higher capacity than the direct link. According to [27], some improvements can be offered by network coding when the relay

is centrally located between the source and destination nodes to assist the users in their data communication. Finally, [28] analyzes the channel capacity of OFDM-based two-hop relaying systems over medium voltage electric power grids and concludes that the DF protocol is superior to the AF one.

A common aspect of some of the aforementioned contributions is the fact that they do not address the low voltage power electric grids, specifically. The remaining ones are based on the use of models for the indoor PLC channel corrupted by additive noise. Although the attained results are appealing in favor of cooperative communication, it is of interest to provide analyses based on measured data to confirm the veracity and usefulness of the results provided so far in the literature.

2.3   HS-OFDM Scheme

The OFDM scheme is a discrete type of modulation in multiple tones consisting of a transmission technique in which the frequency spectrum is divided into a set of parallel sub-channels that are transmitted simultaneously to minimize the effects of frequency selective fading in the channel [3]. Its conception occurred around the 60s, when Chang presented its proposal on the synthesis of orthogonal signals to multiple data transmission channels without causing interference between carriers and inter symbol interference (ISI). After in 1971, Weinstein and Ebert used the discrete Fourier transform (DFT) to reduce the complexity of implementation [29].

However, when the signal passes through a dispersive channel, ISI and inter carrier interference (ICI) appear. These effects can he avoided by inserting a cyclic prefix (CP) between all symbols. The CP is a sort of guard time, removed at the receiver, that consists of the repetition of the last part of the following symbol. Besides using a guard interval in the time domain, it was also necessary to ensure the existence of a perfect orthogonality between the sub-carriers. This scheme only became popular in the 90s with the advent of digital processors. Today, it is adopted in different standards of digital transmission, such as digital audio standards (Digital Audio Broadcasting, Digital Video Broadcasting Terrestrial) together with to the Wi-Fi standards and WiMax wireless networks. In addition to this scheme, the equalization is then easily performed at the frequency domain to compensate the channel attenuation [30].

Usually the term OFDM names the scheme in which a passband data communication is established, while HS-OFDM applies to a baseband data communication. A block diagram of a HS-OFDM scheme is shown in Figure 6, in which $\mathbf{X}_a$ and $\mathbf{Y}_a \in \mathbb{C}^{2N \times 1}$ are frequency domain representation of the transmitted and received signals, respectively.

If the scheme is OFDM, $\mathbf{X}_a = \mathbf{X}$ and the mapping matrix $Map(\cdot)$, represented by Map block, is the identity matrix $\mathbf{I}_N$ of length N, in which N is the number of subcarriers.
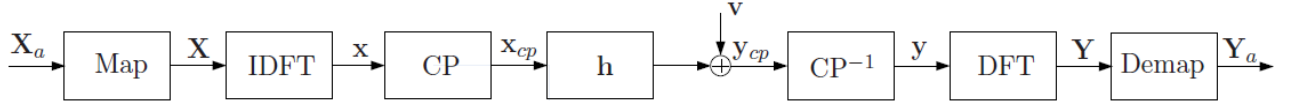
Figure 6: Block diagram of a HS-OFDM scheme.

On the other hand, if the scheme is HS-OFDM then, the mapping process is given by

$$
X[k] = \begin{cases}
\mathbb{R}\{X_a[N-1]\}, & k = 0 \\
X_a[k], & k = 1, \ldots, N-2 \\
\mathbb{I}\{X_a[N-1]\}, & k = N-1 \\
X_a^*[2N-2-k], & k = N, N+1, \ldots, 2N-1
\end{cases}
\tag{2.1}
$$

in which * is the conjugate operator, while $\mathbb{R}\{X[k]\}$ and $\mathbb{I}\{X[k]\}$ refer to real and imaginary part of $X[k]$, respectively. Given $\mathcal{F} = (1/\sqrt{2N})\mathbf{W}$ and $\mathbf{W} \in \mathbb{C}^{2N \times 2N}$, in which $\mathbf{W}$ denotes $2N \times 2N$ DFT matrix, then the vector representation of the transmitted symbol in time domain is given by

$$
\mathbf{x} = \mathcal{F}^\dagger \mathbf{X},
\tag{2.2}
$$

in which $\dagger$ is the conjugate transpose operator. The vector representation of the cyclic prefix is defined by $\mathbf{x}_d \triangleq [x_{2N-1-L_{cp}}\ x_{2N-1-L_{cp}+1}\ \ldots\ x_{2N-1}]^T$, in which T denotes the transpose matrix, L_{cp} is the length of cyclic prefix and x_i is the ith element of vector $\mathbf{x}$. Then $\mathbf{x}_{cp} = [\mathbf{x}_d^T\ \mathbf{x}^T]^T$ and, due to perfect synchronization at the receiver,

$$
\begin{aligned}
\mathbf{y} &= \mathbf{x} \star \mathbf{h} + \mathbf{v} \\
&= \mathbf{C}\mathbf{x} + \mathbf{v}
\end{aligned}
\tag{2.3}
$$

is the output vector resulting from the convolution operation, represented by $\star$, between the HS-OFDM symbol $\mathbf{x}_{cp}$ (transmitted symbol $\mathbf{x}$ extended with the insertion of cyclic prefix) and the vector representation of channel impulse response $\mathbf{h} = [h_0\ h_1 \ldots h_{L_h-1}]^T$, plus the additive noise $\mathbf{v}$. It is considered that $L_{CP} \geq L_h - 1$, then the channel convolution matrix is circulant and given by

$$
\mathbf{C} = \begin{bmatrix}
h_0 & \ldots & 0 & h_{L_h-1} & \ldots & h_1 \\
h_1 & h_0 & \ldots & \ldots & h_{L_h-1} & h_2 \\
h_2 & \ddots & \ddots & \ddots & \ddots & \vdots \\
h_{L_h-1} & \ddots & \ddots & \ddots & \ddots & \vdots \\
0 & h_{L_h-1} & \ddots & \ddots & \ddots & \vdots \\
0 & \ldots & h_{L_h-1} & h_2 & h_1 & h_0
\end{bmatrix}.
\tag{2.4}
$$

Removing the cyclic prefix, it results in

$$\mathbf{y} = \begin{bmatrix} \mathbf{0} & \mathbf{I} \end{bmatrix} \mathbf{y}_{cp}, \tag{2.5}$$

in which $\mathbf{I}_{2N}$ is the identity matrix $2N \times 2N$ and $\mathbf{0}$ is matrix $2N \times L_{CP}$ constituted by zeros. Finally,

$$
\begin{aligned}
\mathcal{F}\mathbf{y} &= \mathcal{F}(\mathbf{C}\mathcal{F}^\dagger \mathbf{X} + \mathbf{v}) \\
\mathbf{Y} &= \mathcal{F}\mathbf{C}\mathcal{F}^\dagger \mathbf{X} + \mathcal{F}\mathbf{v} \\
&= \mathcal{H}\mathbf{X} + \mathbf{V},
\end{aligned}
\tag{2.6}
$$

in which $\mathcal{H} = \mathbf{diag}\{H[0]H[1]\ldots H[2N-1]\}$, $H[k]$ is the k-th coefficient of $\mathbf{H} = \mathcal{F}[\mathbf{h}^T \ \mathbf{0}_{2N-L_h}^T]^T$ and $\mathbf{0}_{2N-L_h}$ is a column vector constituted by $2N - L_h$ zeros.

2.4 Summary

This chapter reviewed some concepts available in the literature about cooperative indoor PLC systems and HS-OFDM scheme.

3 COOPERATIVE INDOOR PLC

This chapter presents some assumptions and a complete mathematical formulation related to the performance of cooperative in-home PLC systems. The presented methodology discusses a comprehensive description of theoretical channel capacity and maximum data rate. The effectiveness of this methodology is validated by using measured power line channels.

To introduce all technical contributions, this chapter is organized as follows: Section 3.1 deals with the calculation of the theoretical channel capacity while Section 3.2 focuses on the maximum data rate when the HS-OFDM scheme is considered.

3.1 Achievable Data Rate

Let $T_C >> 2T_S$, in which T_C and T_S denote the coherence time of a linear PLC channel and the symbol period, respectively. Then the single relay model in which there are a source node (S), a relay node (R) and a destination node (D) is depicted in Figure 7, where $\{h_{SD}[n]\}_{n=0}^{L_{SD}-1}$, $\{h_{SR}[n]\}_{n=0}^{L_{SR}-1}$, and $\{h_{RD}[n]\}_{n=0}^{L_{RD}-1}$ denote the discrete time representation of the LTI impulse responses for the source-destination (SD), source-relay (SR), and relay-destination (RD) links, respectively. Moreover, an equivalent source-relay-destination (SRD) channel impulse response can be represented as $h_{SRD}[n] = h_{SR}[n] \star h_{RD}[n]$, where $L_{SRD} = L_{SR} + L_{RD} - 1$. The data communication is performed in the baseband. We assume that the frequency response of each sub-channel is flat as well as PSD of additive noise.
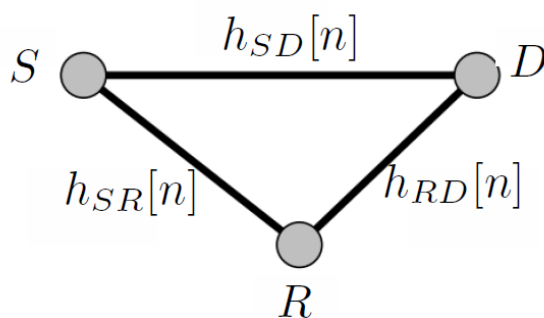
Figure 7: Single relay cooperative model.

The time domain vector representation of the channel impulse responses for SD, SR and RD links can be written as $\mathbf{h}_{SD} = [h_0 h_1 \ldots h_{L_{SD}-1}]^T$, $\mathbf{h}_{SR} = [h_0 h_1 \ldots h_{L_{SR}-1}]^T$, and $\mathbf{h}_{RD} = [h_0 h_1 \ldots h_{L_{RD}-1}]^T$, respectively. Therefore, the vector representation of frequency responses of these channels are $\mathbf{H}_{SD} = \boldsymbol{\mathcal{F}}[\mathbf{h}_{SD}^T \; \mathbf{0}_{2N-L_{SD}}^T]^T$, $\mathbf{H}_{SR} = \boldsymbol{\mathcal{F}}[\mathbf{h}_{SR}^T \; \mathbf{0}_{2N-L_{SR}}^T]^T$, $\mathbf{H}_{RD} = \boldsymbol{\mathcal{F}}[\mathbf{h}_{RD}^T \; \mathbf{0}_{2N-L_{RD}}^T]^T$, in which $\boldsymbol{\mathcal{F}} = (1/\sqrt{2N})\mathbf{W}$. $2N$ is the length of the DFT matrix $\mathbf{W}$ and $\mathbf{0}_L$ is a L-length column vector constituted by zeros. We define $\boldsymbol{\mathcal{H}}_{SD} \triangleq \mathbf{diag}\{H_{SD}[0] \, H_{SD}[1] \, \ldots \, H_{SD}[N-1]\}$, $\boldsymbol{\mathcal{H}}_{SR} \triangleq \mathbf{diag}\{H_{SR}[0] \, H_{SR}[1] \, \ldots \, H_{SR}[N-1]\}$, and

$\boldsymbol{\mathcal{H}}_{RD} \triangleq \mathbf{diag}\{H_{RD}[0]\, H_{RD}[1]\, \ldots\, H_{RD}[N-1]\}$, in which $H_{SD}[k]$, $H_{SR}[k]$ and $H_{RD}[k]$ denote the kth coefficient of $\mathbf{H}_{SD}$, $\mathbf{H}_{SR}$, and $\mathbf{H}_{RD}$, respectively. Due to the fact that the PLC channel is considered LTI, $\boldsymbol{\mathcal{H}}_{SRD} = \boldsymbol{\mathcal{H}}_{SR}\boldsymbol{\mathcal{H}}_{RD}$. It is defined $\boldsymbol{\Lambda}_{|\boldsymbol{\mathcal{H}}_{SD}|^2} \triangleq \mathbf{diag}\{|H_{SD}[0]|^2\, |H_{SD}[1]|^2 \ldots |H_{SD}[N-1]|^2\}$, $\boldsymbol{\Lambda}_{|\boldsymbol{\mathcal{H}}_{SR}|^2} \triangleq \mathbf{diag}\{|H_{SR}[0]|^2\, |H_{SR}[1]|^2\, \ldots\, |H_{SR}[N-1]|^2\}$, and $\boldsymbol{\Lambda}_{|\boldsymbol{\mathcal{H}}_{RD}|^2} \triangleq \mathbf{diag}\{|H_{RD}[0]|^2\, |H_{RD}[1]|^2\, \ldots\, |H_{RD}[N-1]|^2\}$.

The frequency domain representation of a symbol at the S node and the resultant one after the mapping block are $\mathbf{X}_a \in \mathbb{C}^{2N \times 1}$ and $\mathbf{X} \in \mathbb{C}^{N \times 1}$, respectively, such that $\mathbb{E}\{\mathbf{X}\} = 0$, $\mathbb{E}\{\mathbf{XX}^{\dagger}\} = \boldsymbol{\Lambda}_{\sigma_{\mathbf{X}}^2} = \sigma_{\mathbf{X}}^2 \mathbf{I}_N$, where $\sigma_{\mathbf{X}}^2$ is the variance of $X[k]$ (the kth coefficient of the vector $\mathbf{X}$) and $\mathbf{I}_N$ is a N-size identity matrix, $\mathbb{E}\{\cdot\}$ is the expectation operator. Additionally, the frequency domain representation of N-length vectors for the additive noise for SD, SR, RD and SRD links are $\mathbf{V}_{SD}$, $\mathbf{V}_{SR}$, $\mathbf{V}_{RD}$ and $\mathbf{V}_{SRD} = \mathbf{V}_{RD} + \boldsymbol{\mathcal{H}}_{RD}\mathbf{V}_{SR}$. Assume that $\mathbb{E}\{\mathbf{V}_i \odot \mathbf{V}_j\} = \mathbb{E}\{\mathbf{V}_i\} \odot \mathbb{E}\{\mathbf{V}_j\}$, $\forall i \neq j$, in which $\odot$ denotes the Hadamard product and $\mathbb{E}\{\mathbf{V}_i\} = 0$, $i,j \in \{SD, SR, RD\}$ and $\mathbb{E}\{\mathbf{V}_i \mathbf{V}_i^{\dagger}\} = \boldsymbol{\Lambda}_{\sigma_{\mathbf{V}_i}^2} = \mathbf{diag}\{\sigma_{V_i}^2[0]\, \sigma_{V_i}^2[1]\, \ldots\, \sigma_{V_i}^2[N-1]\}$. Then $E\{\mathbf{V}_{SRD}\mathbf{V}_{SRD}^T\} = \boldsymbol{\Lambda}_{\sigma_{\mathbf{V}_{SRD}}^2} = \boldsymbol{\Lambda}_{\sigma_{\mathbf{V}_{RD}}}{}^2 + \boldsymbol{\Lambda}_{\sigma_{\mathbf{V}_{SR}}^2} \boldsymbol{\Lambda}_{|\boldsymbol{\mathcal{H}}_{RD}|^2}$.

Assume that the total power is $P = P_0 + P_1$, where P_0 and P_1 are the powers allocated to the S node and R node to transmit data during the first and the second time slots, respectively. Each slot occupies the same time interval, in other words $T_0 = T_1$, in which T_0 and T_1 are the time intervals allocated to time slot #1 and #2, respectively. The symbol is transmitted by the S node in the first time slot and by the R node in the second time slot, respectively. Perfect synchronization and CSI at the receiver side are considered.

Moreover, it is considered the theoretical channel capacity of the degraded relay channel with ISI and additive colored Gaussian noise as the decomposition into parallel degraded relay channels with individual capacities. Consider that the single relay channel is l-block circular Gaussian relay channel (CGRC) as discussed in [31] (additive noise is a colored Gaussian random process and the LTI PLC channel is frequency selective).

For a single relay channel modeled by a l-CGRC [31] and $\mathbf{X} \in \mathbb{C}^{N \times 1}$ by a zero mean complex Gaussian vector, such that $R_{\mathbf{XX}} = \mathbb{E}\{\mathbf{XX}^{\dagger}\} = \mathbf{I}$, then $\mathbf{Y} \in \mathbb{C}^{2N \times 1}$ is the vectorial frequency domain representation of the received symbol, which is constituted by symbols transmitted through SD and SRD links, given by

$$
\begin{aligned}
\mathbf{Y} &= \begin{bmatrix} \mathbf{Y}_{SD} \\ \mathbf{Y}_{SRD} \end{bmatrix} \\
&= \begin{bmatrix} \boldsymbol{\mathcal{H}}_{SD} & 0 \\ 0 & \boldsymbol{\mathcal{H}}_{SR}\boldsymbol{\mathcal{H}}_{RD} \end{bmatrix} \begin{bmatrix} \boldsymbol{\Lambda}_{\sqrt{P_0}}\mathbf{X} \\ \boldsymbol{\Lambda}_{\sqrt{P_0}}\boldsymbol{\Lambda}_{\sqrt{P_1}}\mathbf{X} \end{bmatrix} + \\
&\quad \begin{bmatrix} \mathbf{V}_{SD} \\ \boldsymbol{\Lambda}_{\sqrt{P_1}}\boldsymbol{\mathcal{H}}_{RD}\mathbf{V}_{SR} + \mathbf{V}_{RD} \end{bmatrix} \\
&= \begin{bmatrix} \boldsymbol{\Lambda}_{\sqrt{P_0}}\boldsymbol{\mathcal{H}}_{SD} & 0 \\ 0 & \boldsymbol{\Lambda}_{\sqrt{P_0}}\boldsymbol{\Lambda}_{\sqrt{P_1}}\boldsymbol{\mathcal{H}}_{SR}\boldsymbol{\mathcal{H}}_{RD} \end{bmatrix} \begin{bmatrix} \mathbf{X} \\ \mathbf{X} \end{bmatrix} + \\
&\quad \begin{bmatrix} \mathbf{I} & 0 & 0 \\ 0 & \boldsymbol{\Lambda}_{\sqrt{P_1}}\boldsymbol{\mathcal{H}}_{RD} & \mathbf{I} \end{bmatrix} \mathbf{V} \\
&= \mathbf{A}\mathbf{X}_1 + \mathbf{B}\mathbf{V}, \tag{3.1}
\end{aligned}
$$

in which $\mathbf{Y}_{SD}$ refers the received symbol through SD link while $\mathbf{Y}_{SRD}$ denotes the received symbol through SRD link; $\mathbf{V} = [\mathbf{V}_{SD}^T\mathbf{V}_{SR}^T\mathbf{V}_{RD}^T]^T$, $\mathbf{X}_1 = [\mathbf{X}^T \ \mathbf{X}^T]^T$, $\boldsymbol{\Lambda}_{\sqrt{P_0}} = \mathbf{diag}\{\sqrt{p_{0,0}}\sqrt{p_{0,1}}\cdots\sqrt{p_{0,N-1}}\}$, $\boldsymbol{\Lambda}_{\sqrt{P_1}} = \mathbf{diag}\{\sqrt{p_{1,0}}\sqrt{p_{1,1}}\cdots\sqrt{p_{1,N-1}}\}$, $\boldsymbol{\Lambda}_{P_0} = \mathbf{diag}\{p_{0,0} \ p_{0,1} \cdots p_{0,N-1}\}$, $\boldsymbol{\Lambda}_{P_1} = \mathbf{diag}\{p_{1,0} \ p_{1,1} \ldots p_{1,N-1}\}$, $\mathrm{Tr}(\boldsymbol{\Lambda}_{P_0}) = P_0$, $\mathrm{Tr}(\boldsymbol{\Lambda}_{P_1}) = P_1$ and $P_0 + P_1 = P$.

Thus, the mutual information between the transmitted and received signals is

$$
\begin{aligned}
I(\mathbf{X}; \mathbf{Y}) &= h(\mathbf{Y}) - h(\mathbf{Y}|\mathbf{X}) \\
&= h(\mathbf{Y}) - (h(\mathbf{A}\mathbf{X}|\mathbf{X}) + h(\mathbf{B}\mathbf{V}|\mathbf{X})) \\
&= h(\mathbf{Y}) - h(\mathbf{B}\mathbf{V}), \tag{3.2}
\end{aligned}
$$

in which $h(\rho)$ refers to the entropy of random variable ρ. Due to the aforementioned assumptions, the received signal $\mathbf{Y}$ is a complex Gaussian vector. Then

$$
h(\mathbf{Y}) = \log_2[(\pi e)^{2N} \det(\mathbf{R}_{\mathbf{YY}})], \tag{3.3}
$$

where the autocorrelation matrix of the received signal is given by

$$
\begin{aligned}
\mathbf{R}_{\mathbf{YY}} &= E\{\mathbf{YY}^\dagger\} \\
&= \mathbf{A}\mathbf{R}_{\mathbf{XX}}\mathbf{A}^\dagger + \mathbf{B}\mathbf{R}_{\mathbf{VV}}\mathbf{B}^\dagger \tag{3.4}
\end{aligned}
$$

where,

$$
\mathbf{A}\mathbf{R}_{\mathbf{XX}}\mathbf{A}^\dagger = \begin{bmatrix} \boldsymbol{\Lambda}_{P_0}\boldsymbol{\Lambda}_{|\boldsymbol{\mathcal{H}}_{SD}|^2} & 0 \\ 0 & \boldsymbol{\Lambda}_{P_0}\boldsymbol{\Lambda}_{P_1}\boldsymbol{\Lambda}_{|\boldsymbol{\mathcal{H}}_{SRD}|^2} \end{bmatrix}
$$

and

$$
\mathbf{B}\mathbf{R}_{\mathbf{VV}}\mathbf{B}^\dagger = \begin{bmatrix} \boldsymbol{\Lambda}_{\sigma_{\mathbf{V}SD^2}} & 0 \\ 0 & \boldsymbol{\Lambda}_{P_1}\boldsymbol{\Lambda}_{|\boldsymbol{\mathcal{H}}_{RD}|^2}\boldsymbol{\Lambda}_{\sigma^2_{\mathbf{V}SR}} + \boldsymbol{\Lambda}_{\sigma^2_{\mathbf{V}RD}} \end{bmatrix}.
$$

Due to the nature of the additive noise (it is an additive colored Gaussian random process), we have

$$h(\mathbf{BV}) = \log_2[(\pi e)^{2N} \det(\mathbf{BR_{VV}B^\dagger})].$$

Next,

$$
\begin{aligned}
I(\mathbf{X}; \mathbf{Y}) &= \log_2[(\pi e)^{2N} \det(\mathbf{AR_{XX}A^\dagger} + \mathbf{BR_{VV}B^\dagger})] - \\
&\quad \log_2[(\pi e)^{2N} \det(\mathbf{BR_{VV}B^\dagger})] \\
&= \log_2\left[\det\left[\mathbf{I} + (\mathbf{AR_{XX}A^\dagger})(\mathbf{BR_{VV}B^\dagger})^{-1}\right]\right]. \tag{3.5}
\end{aligned}
$$

Finally, the theoretical channel capacity of the cooperative channel when AF protocol is applied in the R node is given by

$$C_{AF} = \max_{\mathrm{Tr}(\mathbf{\Lambda}_P) \leq P} \frac{B_w}{2N} \log_2[\det(\mathbf{I} + \mathbf{CD}^{-1})], \tag{3.6}$$

subject to $\mathrm{Tr}(\mathbf{\Lambda}_{P_0}) = P_0$, $\mathrm{Tr}(\mathbf{\Lambda}_{P_1}) = P_1$ and $P_0 + P_1 \leq P$, where $\mathbf{C} = \mathbf{AR_{XX}A^\dagger}$, $\mathbf{D} = \mathbf{BR_{VV}B^\dagger}$ and B_w is the frequency bandwidth.

On the other hand, according to [31], the theoretical channel capacity of the cooperative channel for the DF protocol is given by

$$C_{DF} = \max_{\mathbf{\Lambda}_P, \mathbf{\Lambda}_\alpha} \min\{C_{1,DF}, C_{2,DF}\}, \tag{3.7}$$

in which

$$C_{1,DF} = \frac{B_w}{2N} \log_2[\det(\mathbf{I}_N + \mathbf{\Lambda}_\alpha \mathbf{\Lambda}_{P_0} \mathbf{\Lambda}_{|\mathcal{H}_{\mathcal{SR}}|^2} \mathbf{\Lambda}_{\sigma_{SR}^2}^{-1})] \tag{3.8}$$

and

$$C_{2,DF} = \frac{B_w}{2N} \log_2[\det(\mathbf{I}_N + \mathbf{G})], \tag{3.9}$$

where

$$
\begin{aligned}
\mathbf{G} &= \mathbf{\Lambda}_{\sigma_{SD}^2}^{-1}\Big(\mathbf{\Lambda}_{|\mathcal{H}_{SD}|^2}\mathbf{\Lambda}_{P_0} + \mathbf{\Lambda}_{|\mathcal{H}_{RD}|^2}\mathbf{\Lambda}_{P_1} + \\
&\quad 2\sqrt{\mathbf{\Lambda}_{\bar{\alpha}}\mathbf{\Lambda}_{|\mathcal{H}_{SD}\mathcal{H}_{RD}|^2}\mathbf{\Lambda}_{P_0}\mathbf{\Lambda}_{P_1}}\Big), \tag{3.10}
\end{aligned}
$$

$\mathbf{\Lambda}_{\bar{\alpha}} = \mathbf{I}_N - \mathbf{\Lambda}_\alpha$ and $\mathbf{\Lambda}_\alpha$ is the cross-correlation matrix between the signals sent by the S and R nodes.

3.2   Maximum Data Rate of a HS-OFDM Scheme

To evaluate the maximum data rate of a HS-OFDM scheme it is assumed perfect synchronization and CSI available at all nodes. Concerning the HS-OFDM scheme and the combining techniques, if the AF protocol is considered, then the length of the CP of the transmitted symbol is $L_{CP} \geq \max\{L_{SD} - 1, L_{SR} + L_{RD} - 2\}$. On the other hand,

for the DF protocol, in the first time slot, the source broadcasts data to the relay and destination and, then, the relay transmits the detected data to the destination in the second time slot [32]. In this case, $L_{CP} \geq \max\{L_{SD} - 1, L_{SR} - 1\}$ in the first time slot and $L_{CP} \geq L_{RD} - 1$ for the second time slot.

For the combining techniques, the coefficients of the weighting factor matrix $\mathbf{D}_{a,b,c} = \mathbf{diag}\{|\alpha_{a,b,c}[0]|, |\alpha_{a,b,c}[1]|, \ldots, |\alpha_{a,b,c}[N-1]|\}$, $a \in \{\text{EGC,SC,MRC}\}$, $b \in \{\text{AF,DF}\}$ and $c \in \{\text{SD,SRD}\}$ can be represented, for the EGC technique, by

$$\alpha_{EGC,b,c}[k] = \frac{1}{2}, \tag{3.11}$$

in which $\phi_c[k] = \arg\{H_c[k]\}$. By applying the SC technique, we may write

$$\alpha_{SC,b,SD}[k] = \begin{cases} 1, & \text{if } \Lambda_{\gamma_{SD}}[k,k] \geq \Lambda_{\gamma_{b,SRD}}[k,k] \\ 0, & \text{otherwise} \end{cases} \tag{3.12}$$

$$\alpha_{SC,b,SRD}[k] = \begin{cases} 1, & \text{if } \Lambda_{\gamma_{b,SRD}}[k,k] > \Lambda_{\gamma_{SD}}[k,k] \\ 0, & \text{otherwise.} \end{cases} \tag{3.13}$$

in which $\Lambda_{\gamma_{SD}}[k,k]$ and $\Lambda_{\gamma_{b,SRD}}[k,k]$ denote the (k,k) element of the normalized SNR matrices $\mathbf{\Lambda}_{\gamma_{SD}}$ and $\mathbf{\Lambda}_{\gamma_{b,SRD}}$, respectively. Finally, the use of the MRC technique assumes that

$$\alpha_{MRC,b,SD}[k] = \frac{\mathbf{\Lambda}_{\gamma_{SD}}(k,k)}{\mathbf{\Lambda}_{\gamma_{SD}}(k,k) + \mathbf{\Lambda}_{\gamma_{b,SRD}}(k,k)}, \tag{3.14}$$

and

$$\alpha_{MRC,b,SRD}[k] = \frac{\mathbf{\Lambda}_{\gamma_{b,SRD}}(k,k)}{\mathbf{\Lambda}_{\gamma_{SD}}(k,k) + \mathbf{\Lambda}_{\gamma_{b,SRD}}(k,k)}, \tag{3.15}$$

where $\mathbf{\Lambda}_{\gamma_{SD}}(k,k)$ and $\mathbf{\Lambda}_{\gamma_{b,SRD}}(k,k)$ are, respectively the (k,k) element of $\mathbf{\Lambda}_{\gamma_{SD}}$ and $\mathbf{\Lambda}_{\gamma_{b,SRD}}$, which are normalized SNR matrices defined according to the HS-OFDM schemes; see Sections 3.3 and 3.4. Note that all SNR matrices are diagonal, therefore, $\frac{\mathbf{\Lambda}_{num}}{\mathbf{\Lambda}_{den}} = \mathbf{\Lambda}_{num}\mathbf{\Lambda}_{den}^{-1}$, in which $\mathbf{\Lambda}_{num}$ and $\mathbf{\Lambda}_{den}$ represent the numerator and denominator matrices, respectively.

Due to the fact that the in-home PLC channels are frequency selective, the additive noise is a colored Gaussian random process and the transmitted signal is assumed to be a Gaussian random process; thus, the maximum data rate can be evaluated by using

$$C_\beta = \max_{\mathbf{\Lambda}_P} \frac{B_w}{2(N + L_{CP})} \sum_{k=0}^{N-1} \log_2\left[1 + \mathbf{\Lambda}_{\gamma_\beta}(k,k)\right], \tag{3.16}$$

subject to $\text{Tr}(\mathbf{\Lambda}_{P_0}) = P_0$, $\text{Tr}(\mathbf{\Lambda}_{P_1}) = P_1$ and $P_0 + P_1 \leq P$, in which $\beta \in \{\text{SD,AF-SRD,DF-SRD,AF-EGC,DF-EGC,AF-SC,DF-SC,AF-MRC,DF-MRC}\}$ for the HS-OFDM scheme.

3.3 HS-OFDM with FDE-ZF

In this section, it is described the maximum data rate of an HS-OFDM scheme that makes use of FDE based on ZF, AF/DF protocols and EGC/SC/MRC techniques, when the single relay model is considered.

The FDE-ZF applies the inverse of the channel frequency response to the received signal, and so, the expression for the d link is $\mathcal{H}_d^{-1}$. Regarding the vectorial representation of the channel output at the time domain is given by

$$\mathbf{y}_{SD} = \mathbf{\Lambda}_{\sqrt{P_0}}\mathbf{C}_{SD}\mathbf{x} + \mathbf{v}_{SD}. \tag{3.17}$$

The vector frequency domain representation of (3.17) is given by

$$
\begin{aligned}
\mathbf{Y}_{SD} &= \mathcal{F}\mathbf{y}_{SD} \\
&= \mathbf{\Lambda}_{\sqrt{P_0}}\mathcal{H}_{SD}\mathbf{X} + \mathbf{V}_{SD}.
\end{aligned}
\tag{3.18}
$$

Finally the estimate of the transmitted symbol is given by

$$
\begin{aligned}
\hat{\mathbf{X}}_{SD} &= \mathcal{H}_{SD}^{-1}\mathbf{Y}_{SD} \\
&= \mathbf{\Lambda}_{\sqrt{P_0}}\mathbf{X} + \mathcal{H}_{SD}^{-1}\mathbf{V}_{SD} \\
&= \mathbf{Z} + \mathbf{V}_{SD}.
\end{aligned}
\tag{3.19}
$$

Evaluating,

$$\mathbb{E}\{\mathbf{Z}\mathbf{Z}^{\dagger}\} = \mathbf{\Lambda}_{P_0}\mathbf{\Lambda}_{\sigma_X^2} \tag{3.20}$$

and

$$\mathbb{E}\{\mathbf{V}_{SD}\mathbf{V}_{SD}^{\dagger}\} = \mathbf{\Lambda}_{|\mathcal{H}_{SD}|^2}^{-1}\mathbf{\Lambda}_{\sigma_{V_{SD}}^2}. \tag{3.21}$$

So, we obtain a SNR matrix, which is given by

$$
\begin{aligned}
\mathbf{\Lambda}_{\gamma_{SD}} &= \frac{\mathbb{E}\{\mathbf{Z}\mathbf{Z}^{\dagger}\}}{\mathbb{E}\{\mathbf{V}_{SD}\mathbf{V}_{SD}^{\dagger}\}} \\
&= \frac{\mathbf{\Lambda}_{P_0}\mathbf{\Lambda}_{\sigma_X^2}}{\mathbf{\Lambda}_{|\mathcal{H}_{SD}|^2}^{-1}\mathbf{\Lambda}_{\sigma_{V_{SD}}^2}},
\end{aligned}
\tag{3.22}
$$

which is equal to the normalized SNR matrix because $\mathbf{\Lambda}_{\sigma_X^2} = \mathbf{I}$. Note that $\mathbb{E}\{\mathbf{Z}\mathbf{Z}^{\dagger}\}$ and $\mathbb{E}\{\mathbf{V}_{SD}\mathbf{V}_{SD}^{\dagger}\}$ are diagonal matrices.

For the AF protocol, the channel output at the frequency domain through the relay node is given by

$$\mathbf{Y}_{AF,SRD} = \Lambda_{\sqrt{P_0}} \Lambda_{\sqrt{P_1}} \mathcal{H}_{SRD} \mathbf{X} + \Lambda_{\sqrt{P_1}} \mathcal{H}_{RD} \mathbf{V}_{SR} + \mathbf{V}_{RD}. \tag{3.23}$$

Then, an estimate of the transmitted symbol is given by

$$\begin{aligned}
\hat{\mathbf{X}}_{AF,SRD} &= \mathcal{H}_{SRD}^{-1} \mathbf{Y}_{AF,SRD} \\
&= \Lambda_{\sqrt{P_0}} \Lambda_{\sqrt{P_1}} \mathbf{X} + \Lambda_{\sqrt{P_1}} \mathcal{H}_{SR}^{-1} \mathbf{V}_{SR} + \mathcal{H}_{SRD}^{-1} \mathbf{V}_{RD} \\
&= \mathbf{Z} + \mathbf{V}_{SRD}.
\end{aligned} \tag{3.24}$$

Finally, the SNR matrix for the SRD link when the AF protocol is applied is expressed by

$$\begin{aligned}
\Lambda_{\gamma_{AF,SRD}} &= \frac{\mathbb{E}\{\mathbf{Z}\mathbf{Z}^{\dagger}\}}{\mathbb{E}\{\mathbf{V}_{SRD}\mathbf{V}_{SRD}^{\dagger}\}} \\
&= \frac{\Lambda_{P_0} \Lambda_{P_1} \Lambda_{\sigma_{\mathbf{X}}^2}}{\Lambda_{P_1} \Lambda_{|\mathcal{H}_{SR}|^2}^{-1} \Lambda_{\sigma_{\mathbf{V}_{SR}}^2} + \Lambda_{|\mathcal{H}_{SRD}|^2}^{-1} \Lambda_{\sigma_{\mathbf{V}_{RD}}^2}}.
\end{aligned} \tag{3.25}$$

On the other hand, the use of the DF protocol results in a vectorial representation of the channel output and an estimate of the transmitted symbol through the SRD link given by, respectively,

$$\mathbf{Y}_{DF,SRD} = \Lambda_{\sqrt{P_1}} \mathcal{H}_{RD} \mathbf{X} + \Lambda_{\sqrt{P_1}} \mathcal{H}_{RD} \mathbf{E} + \mathbf{V}_{RD} \tag{3.26}$$

where $\mathbf{E}$ denotes the error introduced by the erroneous symbol detection performed at the R node and

$$\begin{aligned}
\hat{\mathbf{X}}_{DF,SRD} &= \mathcal{H}_{RD}^{-1} \mathbf{Y}_{DF,SRD} \\
&= \Lambda_{\sqrt{P_1}} \mathbf{X} + \Lambda_{\sqrt{P_1}} \mathbf{E} + \mathcal{H}_{RD}^{-1} \mathbf{V}_{RD} \\
&= \mathbf{Z} + \mathbf{V}_{SRD}.
\end{aligned} \tag{3.27}$$

So, the SNR matrix is expressed by

$$\begin{aligned}
\Lambda_{\gamma_{DF,SRD}} &= \frac{\mathbb{E}\{\mathbf{Z}\mathbf{Z}^{\dagger}\}}{\mathbb{E}\{\mathbf{V}_{SRD}\mathbf{V}_{SRD}^{\dagger}\}} \\
&= \frac{\Lambda_{P_1} \Lambda_{\sigma_{\mathbf{X}}^2}}{\Lambda_{P_1} \Lambda_{\sigma_{\mathbf{E}}^2} + \Lambda_{|\mathcal{H}_{RD}|^2}^{-1} \Lambda_{\sigma_{\mathbf{V}_{RD}}^2}}.
\end{aligned} \tag{3.28}$$

The use of EGC, SC, and MRC techniques together with the AF protocol results in a final estimate of the transmitted symbol and the SNR matrix, which are given by, respectively

$$
\begin{aligned}
\hat{\mathbf{X}}_{a,AF} &= \mathbf{D}_{a,b,SD}\hat{\mathbf{X}}_{SD} + \mathbf{D}_{a,b,SRD}\hat{\mathbf{X}}_{AF,SRD} \\
&= \left(\mathbf{\Lambda}_{\sqrt{P_0}}\mathbf{D}_{a,b,SD} + \mathbf{\Lambda}_{\sqrt{P_0}}\mathbf{\Lambda}_{\sqrt{P_1}}\mathbf{D}_{a,b,SRD}\right)\mathbf{X} + \mathbf{D}_{a,b,SD}\boldsymbol{\mathcal{H}}_{SD}^{-1}\mathbf{V}_{SD} + \\
&\qquad \mathbf{D}_{a,b,SRD}(\mathbf{\Lambda}_{\sqrt{P_1}}\boldsymbol{\mathcal{H}}_{SR}^{-1}\mathbf{V}_{SR} + \boldsymbol{\mathcal{H}}_{SRD}^{-1}\mathbf{V}_{RD}) \\
&= \mathbf{Z} + \mathbf{V}_{SRD}
\end{aligned}
\tag{3.29}
$$

and

$$
\begin{aligned}
\mathbf{\Lambda}_{\gamma_{a,AF}} &= \frac{\mathbb{E}\{\mathbf{Z}\mathbf{Z}^{\dagger}\}}{\mathbb{E}\{\mathbf{V}_{SRD}\mathbf{V}_{SRD}^{\dagger}\}} \\
&= \frac{\left|\mathbf{\Lambda}_{\sqrt{P_0}}\mathbf{D}_{a,b,SD} + \mathbf{\Lambda}_{\sqrt{P_0}}\mathbf{\Lambda}_{\sqrt{P_1}}\mathbf{D}_{a,b,SRD}\right|^2 \mathbf{\Lambda}_{\sigma_{\mathbf{X}}^2}}{\mathbf{\Lambda}_{|\boldsymbol{\mathcal{H}}_{SD}|^2}^{-1}\mathbf{\Lambda}_{\sigma_{\mathbf{V}_{SD}}^2}\mathbf{D}_{a,b,SD}^2 + (\mathbf{\Lambda}_{P_1}\mathbf{\Lambda}_{|\boldsymbol{\mathcal{H}}_{SR}|^2}\mathbf{\Lambda}_{\sigma_{\mathbf{V}_{SR}}^2} + \mathbf{\Lambda}_{|\boldsymbol{\mathcal{H}}_{SRD}|^2}^{-1}\mathbf{\Lambda}_{\sigma_{\mathbf{V}_{RD}}^2})\mathbf{D}_{a,b,SRD}^2}
\end{aligned}
\tag{3.30}
$$

The use of EGC, SC, and MRC techniques together with the DF protocol results in a final estimate of the transmitted symbol and the correspondent SNR matrix, which are given by

$$
\begin{aligned}
\hat{\mathbf{X}}_{a,DF} &= \mathbf{D}_{a,b,SD}\hat{\mathbf{X}}_{SD} + \mathbf{D}_{a,b,SRD}\hat{\mathbf{X}}_{DF,SRD} \\
&= \left(\mathbf{\Lambda}_{\sqrt{P_0}}\mathbf{D}_{a,b,SD} + \mathbf{\Lambda}_{\sqrt{P_1}}\mathbf{D}_{a,b,SRD}\right)\mathbf{X} + \mathbf{D}_{a,b,SD}\boldsymbol{\mathcal{H}}_{SD}^{-1}\mathbf{V}_{SD} + \\
&\qquad \mathbf{D}_{a,b,SRD}(\mathbf{\Lambda}_{\sqrt{P_1}}\mathbf{E} + \boldsymbol{\mathcal{H}}_{RD}^{-1}\mathbf{V}_{RD}) \\
&= \mathbf{Z} + \mathbf{V}_{SRD}
\end{aligned}
\tag{3.31}
$$

and

$$
\begin{aligned}
\mathbf{\Lambda}_{\gamma_{a,DF}} &= \frac{\mathbb{E}\{\mathbf{Z}\mathbf{Z}^{\dagger}\}}{\mathbb{E}\{\mathbf{V}_{SRD}\mathbf{V}_{SRD}^{\dagger}\}} \\
&= \frac{\left|\mathbf{\Lambda}_{\sqrt{P_0}}\mathbf{D}_{a,b,SD} + \mathbf{\Lambda}_{\sqrt{P_1}}\mathbf{D}_{a,b,SRD}\right|^2 \mathbf{\Lambda}_{\sigma_{\mathbf{X}}^2}}{\mathbf{\Lambda}_{|\boldsymbol{\mathcal{H}}_{SD}|^2}^{-1}\mathbf{\Lambda}_{\sigma_{\mathbf{V}_{SD}}^2}\mathbf{D}_{a,b,SD}^2 + \left(\mathbf{\Lambda}_{\sqrt{P_1}}\mathbf{\Lambda}_{\sigma_{\mathbf{E}}^2} + \mathbf{\Lambda}_{|\boldsymbol{\mathcal{H}}_{RD}|^2}^{-1}\mathbf{\Lambda}_{\sigma_{\mathbf{V}_{RD}}^2}\right)\mathbf{D}_{a,b,SRD}^2}
\end{aligned}
\tag{3.32}
$$

3.4 HS-OFDM with FDE-MMSE

In this section, it is described the maximum data rate of an HS-OFDM scheme that makes use of FDE based on MMSE, AF/DF protocols and EGC/SC/MRC techniques, when the single relay model is considered.

For the FDE-MMSE, applied to the d link, the equalizer expression is $\boldsymbol{\mathcal{H}}_d^{\dagger}/(\boldsymbol{\mathcal{H}}_d^{\dagger}\boldsymbol{\mathcal{H}}_d + \frac{\mathbf{\Lambda}_{\sigma_{\mathbf{V}_d}^2}}{\mathbf{P}_{\mathbf{x}}\mathbf{\Lambda}_{\sigma_{\mathbf{X}}^2}})$, in which $\mathbf{P}_{\mathbf{x}}$ is the power allocation matrix applied to the subcarriers of the HS-OFDM symbol $\left(\mathbf{P}_{\mathbf{x}} \in \{\mathbf{\Lambda}_{\sqrt{P_0}}, \mathbf{\Lambda}_{\sqrt{P_1}}\}\right)$. Regarding the vectorial representation of the channel output at the frequency domain is given by

$$
\mathbf{Y}_{SD} = \mathbf{\Lambda}_{\sqrt{P_0}}\boldsymbol{\mathcal{H}}_{SD}\mathbf{X} + \mathbf{V}_{SD}.
\tag{3.33}
$$

A estimate of the transmitted symbol is given by

$$
\begin{aligned}
\hat{\mathbf{X}}_{SD} &= \frac{\boldsymbol{\mathcal{H}}_{SD}^{\dagger}}{\boldsymbol{\Lambda}_{|\boldsymbol{\mathcal{H}}_{SD}|^2} + \frac{\boldsymbol{\Lambda}_{\sigma_{\mathbf{V}_{SD}}^2}}{\boldsymbol{\Lambda}_{P_0}\boldsymbol{\Lambda}_{\sigma_{\mathbf{X}}^2}}} \mathbf{Y}_{SD} \\
&= \frac{\boldsymbol{\Lambda}_{\sqrt{P_0}}\boldsymbol{\Lambda}_{|\boldsymbol{\mathcal{H}}_{SD}|^2}\mathbf{X}}{\boldsymbol{\Lambda}_{|\boldsymbol{\mathcal{H}}_{SD}|^2} + \frac{\boldsymbol{\Lambda}_{\sigma_{\mathbf{V}_{SD}}^2}}{\boldsymbol{\Lambda}_{P_0}\boldsymbol{\Lambda}_{\sigma_{\mathbf{X}}^2}}} + \frac{\boldsymbol{\mathcal{H}}_{SD}^{\dagger}\mathbf{V}_{SD}}{\boldsymbol{\Lambda}_{|\boldsymbol{\mathcal{H}}_{SD}|^2} + \frac{\boldsymbol{\Lambda}_{\sigma_{\mathbf{V}_{SD}}^2}}{\boldsymbol{\Lambda}_{P_0}\boldsymbol{\Lambda}_{\sigma_{\mathbf{X}}^2}}} \\
&= \mathbf{Z} + \mathbf{V}_{SD}.
\end{aligned}
\tag{3.34}
$$

Finally, we obtain a SNR matrix, which is given by

$$
\begin{aligned}
\boldsymbol{\Lambda}_{\gamma_{SD}} &= \frac{\mathbb{E}\{\mathbf{Z}\mathbf{Z}^{\dagger}\}}{\mathbb{E}\{\mathbf{V}_{SD}\mathbf{V}_{SD}^{\dagger}\}} \\
&= \frac{\boldsymbol{\Lambda}_{P_0}\boldsymbol{\Lambda}_{|\boldsymbol{\mathcal{H}}_{SD}|^2}}{\boldsymbol{\Lambda}_{\sigma_{\mathbf{V}_{SD}}^2}}\boldsymbol{\Lambda}_{\sigma_{\mathbf{X}}^2}.
\end{aligned}
\tag{3.35}
$$

For the AF protocol, an estimate of the transmitted symbol through the relay node is given by

$$
\begin{aligned}
\hat{\mathbf{X}}_{AF,SRD} &= \frac{\boldsymbol{\Lambda}_{\sqrt{P_0}}\boldsymbol{\Lambda}_{\sqrt{P_1}}\boldsymbol{\Lambda}_{|\boldsymbol{\mathcal{H}}_{SRD}|^2}\mathbf{X}}{\boldsymbol{\Lambda}_{|\boldsymbol{\mathcal{H}}_{SRD}|^2} + \frac{\boldsymbol{\Lambda}_{\sigma_{\mathbf{V}_{SRD}}^2}}{\boldsymbol{\Lambda}_{P_0}\boldsymbol{\Lambda}_{P_1}\boldsymbol{\Lambda}_{\sigma_{\mathbf{X}}^2}}} + \frac{\boldsymbol{\Lambda}_{\sqrt{P_1}}\boldsymbol{\mathcal{H}}_{SRD}^{\dagger}\boldsymbol{\mathcal{H}}_{RD}^{\dagger}\mathbf{V}_{SR}}{\boldsymbol{\Lambda}_{|\boldsymbol{\mathcal{H}}_{SRD}|^2} + \frac{\boldsymbol{\Lambda}_{\sigma_{\mathbf{V}_{SRD}}^2}}{\boldsymbol{\Lambda}_{P_0}\boldsymbol{\Lambda}_{P_1}\boldsymbol{\Lambda}_{\sigma_{\mathbf{X}}^2}}} + \\
&\qquad \frac{\boldsymbol{\mathcal{H}}_{SRD}^{\dagger}\mathbf{V}_{RD}}{\boldsymbol{\Lambda}_{|\boldsymbol{\mathcal{H}}_{SRD}|^2} + \frac{\boldsymbol{\Lambda}_{\sigma_{\mathbf{V}_{SRD}}^2}}{\boldsymbol{\Lambda}_{P_0}\boldsymbol{\Lambda}_{P_1}\boldsymbol{\Lambda}_{\sigma_{\mathbf{X}}^2}}} \\
&= \mathbf{Z} + \mathbf{V}_{SRD}.
\end{aligned}
\tag{3.36}
$$

Finally, the SNR matrix for the SRD link when the AF protocol is applied is expressed by

$$
\begin{aligned}
\boldsymbol{\Lambda}_{\gamma_{AF,SRD}} &= \frac{\mathbb{E}\{\mathbf{Z}\mathbf{Z}^{\dagger}\}}{\mathbb{E}\{\mathbf{V}_{SRD}\mathbf{V}_{SRD}^{\dagger}\}} \\
&= \frac{\boldsymbol{\Lambda}_{P_0}\boldsymbol{\Lambda}_{P_1}\boldsymbol{\Lambda}_{|\boldsymbol{\mathcal{H}}_{SRD}|^2}\boldsymbol{\Lambda}_{\sigma_{\mathbf{X}}^2}}{\boldsymbol{\Lambda}_{P_1}\boldsymbol{\Lambda}_{|\boldsymbol{\mathcal{H}}_{RD}|^2}\boldsymbol{\Lambda}_{\sigma_{\mathbf{V}_{SR}}}^2 + \boldsymbol{\Lambda}_{\sigma_{\mathbf{V}_{RD}}^2}}
\end{aligned}
\tag{3.37}
$$

On the other hand, the use of the DF protocol results in an estimate of the transmitted symbol and the SNR matrix through the SRD link given by, respectively,

$$
\begin{aligned}
\hat{\mathbf{X}}_{DF,SRD} &= \frac{\boldsymbol{\Lambda}_{\sqrt{P_1}}\boldsymbol{\Lambda}_{|\boldsymbol{\mathcal{H}}_{RD}|^2}}{\boldsymbol{\Lambda}_{|\boldsymbol{\mathcal{H}}_{RD}|^2} + \frac{\boldsymbol{\Lambda}_{\sigma_{\mathbf{V}_{RD}}^2}}{\boldsymbol{\Lambda}_{P_1}\boldsymbol{\Lambda}_{\sigma_{\mathbf{X}}^2}}}\mathbf{X} + \frac{\boldsymbol{\Lambda}_{\sqrt{P_1}}\boldsymbol{\Lambda}_{|\boldsymbol{\mathcal{H}}_{RD}|^2}}{\boldsymbol{\Lambda}_{|\boldsymbol{\mathcal{H}}_{RD}|^2} + \frac{\boldsymbol{\Lambda}_{\sigma_{\mathbf{V}_{RD}}^2}}{\boldsymbol{\Lambda}_{P_1}\boldsymbol{\Lambda}_{\sigma_{\mathbf{X}}^2}}}\mathbf{E} + \qquad (3.38) \\
&\qquad \frac{\boldsymbol{\mathcal{H}}_{RD}^{\dagger}}{\boldsymbol{\Lambda}_{|\boldsymbol{\mathcal{H}}_{RD}|^2} + \frac{\boldsymbol{\Lambda}_{\sigma_{\mathbf{V}_{RD}}^2}}{\boldsymbol{\Lambda}_{P_1}\boldsymbol{\Lambda}_{\sigma_{\mathbf{X}}^2}}}\mathbf{V}_{RD} \\
&= \mathbf{Z} + \mathbf{V}_{SRD}
\end{aligned}
\tag{3.39}
$$

and

$$
\begin{aligned}
\mathbf{\Lambda}_{\gamma_{DF,SRD}} &= \frac{\mathbb{E}\{\mathbf{Z}\mathbf{Z}^\dagger\}}{\mathbb{E}\{\mathbf{V}_{SRD}\mathbf{V}_{SRD}^\dagger\}} \\
&= \frac{\mathbf{\Lambda}_{P_1}\mathbf{\Lambda}_{|\mathcal{H}_{RD}|^2}\mathbf{\Lambda}_{\sigma_\mathbf{X}^2}}{\mathbf{\Lambda}_{P_1}\mathbf{\Lambda}_{|\mathcal{H}_{RD}|^2}\mathbf{\Lambda}_{\sigma_\mathbf{E}}^2 + \mathbf{\Lambda}_{\sigma_{\mathbf{V}_{RD}}^2}}.
\end{aligned}
\tag{3.40}
$$

The use of EGC, SC, and MRC techniques together with the AF protocol results in a final estimate of the transmitted symbol and its correspondent SNR matrix, which are given by

$$
\begin{aligned}
\hat{\mathbf{X}}_{a,AF} &= \mathbf{D}_{a,b,SD}\hat{\mathbf{X}}_{SD} + \mathbf{D}_{a,b,SRD}\hat{\mathbf{X}}_{AF,SRD} \\
&= \left(\frac{\mathbf{\Lambda}_{\sqrt{P_0}}\mathbf{D}_{a,b,SD}\mathbf{\Lambda}_{|\mathcal{H}_{SD}|^2}}{\mathbf{\Lambda}_{|\mathcal{H}_{SD}|^2} + \frac{\mathbf{\Lambda}_{\sigma_{\mathbf{V}_{SD}}^2}}{\mathbf{\Lambda}_{P_0}\mathbf{\Lambda}_{\sigma_\mathbf{X}^2}}} + \frac{\mathbf{\Lambda}_{\sqrt{P_0}}\mathbf{\Lambda}_{\sqrt{P_1}}\mathbf{D}_{a,b,SRD}\mathbf{\Lambda}_{|\mathcal{H}_{SRD}|^2}}{(\mathbf{\Lambda}_{|\mathcal{H}_{SRD}|^2} + \frac{\mathbf{\Lambda}_{\sigma_{\mathbf{V}_{SR}}^2}}{\mathbf{\Lambda}_{P_0}\mathbf{\Lambda}_{\sigma_\mathbf{X}^2}})(\mathbf{\Lambda}_{|\mathcal{H}_{RD}|^2} + \frac{\mathbf{\Lambda}_{\sigma_{\mathbf{V}_{RD}}^2}}{\mathbf{\Lambda}_{P_1}\mathbf{\Lambda}_{\sigma_\mathbf{X}^2}})} \right)\mathbf{X} + \\
&\quad \frac{\mathbf{D}_{a,b,SD}\mathcal{H}_{SD}^\dagger \mathbf{V}_{SD}}{\mathbf{\Lambda}_{|\mathcal{H}_{SD}|^2} + \frac{\mathbf{\Lambda}_{\sigma_{\mathbf{V}_{SD}}^2}}{\mathbf{\Lambda}_{P_0}\mathbf{\Lambda}_{\sigma_\mathbf{X}^2}}} + \frac{\mathbf{\Lambda}_{\sqrt{P_1}}\mathbf{D}_{a,b,SRD}\mathbf{\Lambda}_{\mathcal{H}_{RD}^\dagger}\mathbf{\Lambda}_{\mathcal{H}_{SRD}^\dagger}\mathbf{V}_{SR}}{\mathbf{\Lambda}_{|\mathcal{H}_{SRD}|^2} + \frac{\mathbf{\Lambda}_{\sigma_{\mathbf{V}_{SR}}^2}}{\mathbf{\Lambda}_{P_0}\mathbf{\Lambda}_{P_1}\mathbf{\Lambda}_{\sigma_\mathbf{X}^2}}} + \\
&\quad \frac{\mathbf{D}_{a,b,SRD}\mathbf{\Lambda}_{|\mathcal{H}_{SRD}|^2}\mathbf{V}_{RD}}{\mathbf{\Lambda}_{|\mathcal{H}_{SRD}|^2} + \frac{\mathbf{\Lambda}_{\sigma_{\mathbf{V}_{SRD}}^2}}{\mathbf{\Lambda}_{P_0}\mathbf{\Lambda}_{P_1}\mathbf{\Lambda}_{\sigma_\mathbf{X}^2}}} \\
&= \mathbf{Z} + \mathbf{V}_{SRD}
\end{aligned}
\tag{3.41}
$$

and

$$
\mathbf{\Lambda}_{\gamma_{a,AF}} = \frac{\mathbb{E}\{\mathbf{Z}\mathbf{Z}^\dagger\}}{\mathbb{E}\{\mathbf{V}_{SRD}\mathbf{V}_{SRD}^\dagger\}}
\tag{3.42}
$$

$$
= \frac{\left(\frac{\mathbf{\Lambda}_{\sqrt{P_0}}\mathbf{D}_{a,b,SD}\mathbf{\Lambda}_{|\mathcal{H}_{SD}|^2}}{\mathbf{\Lambda}_{|\mathcal{H}_{SD}|^2} + \frac{\mathbf{\Lambda}_{\sigma_{\mathbf{V}_{SD}}^2}}{\mathbf{\Lambda}_{P_0}\mathbf{\Lambda}_{\sigma_\mathbf{X}^2}}} + \frac{\mathbf{\Lambda}_{\sqrt{P_0}}\mathbf{\Lambda}_{\sqrt{P_1}}\mathbf{D}_{a,b,SRD}\mathbf{\Lambda}_{|\mathcal{H}_{SRD}|^2}}{\mathbf{\Lambda}_{|\mathcal{H}_{SRD}|^2} + \frac{\mathbf{\Lambda}_{\sigma_{\mathbf{V}_{SRD}}^2}}{\mathbf{\Lambda}_{P_0}\mathbf{\Lambda}_{P_1}\mathbf{\Lambda}_{\sigma_\mathbf{X}^2}}} \right)^2 \mathbf{\Lambda}_{\sigma_\mathbf{X}^2}}{\frac{\mathbf{\Lambda}_{|\mathcal{H}_{SD}|^2}\mathbf{\Lambda}_{\sigma_{\mathbf{V}_{SD}}^2}\mathbf{D}_{a,b,SD}^2}{\left(\mathbf{\Lambda}_{|\mathcal{H}_{SD}|^2} + \frac{\mathbf{\Lambda}_{\sigma_{\mathbf{V}_{SD}}^2}}{\mathbf{\Lambda}_{P_0}\mathbf{\Lambda}_{\sigma_\mathbf{X}^2}}\right)^2} + \frac{\mathbf{\Lambda}_{|\mathcal{H}_{SRD}|^2}\mathbf{\Lambda}_{\sigma_{\mathbf{V}_{RD}}^2}\mathbf{D}_{a,b,SRD}^2}{\left(\mathbf{\Lambda}_{|\mathcal{H}_{SRD}|^2} + \frac{\mathbf{\Lambda}_{\sigma_{\mathbf{V}_{SRD}}^2}}{\mathbf{\Lambda}_{P_0}\mathbf{\Lambda}_{P_1}\mathbf{\Lambda}_{\sigma_\mathbf{X}^2}}\right)^2} + \frac{\mathbf{\Lambda}_{P_1}\mathbf{\Lambda}_{|\mathcal{H}_{SRD}|^2}\mathbf{\Lambda}_{|\mathcal{H}_{RD}|^2}\mathbf{\Lambda}_{\sigma_{\mathbf{V}_{SR}}^2}\mathbf{D}_{a,b,SRD}^2}{\left(\mathbf{\Lambda}_{|\mathcal{H}_{SRD}|^2} + \frac{\mathbf{\Lambda}_{\sigma_{\mathbf{V}_{SRD}}^2}}{\mathbf{\Lambda}_{P_0}\mathbf{\Lambda}_{P_1}\mathbf{\Lambda}_{\sigma_\mathbf{X}^2}}\right)^2}}.
$$

For the DF protocol, the final estimate of the transmitted symbol and its correspondent SNR matrix are given by

$$
\begin{aligned}
\hat{\mathbf{X}}_{a,DF} &= \mathbf{D}_{a,b,SD}\hat{\mathbf{X}}_{SD} + \mathbf{D}_{a,b,SRD}\hat{\mathbf{X}}_{DF,SRD} \\
&= \left(\frac{\mathbf{D}_{a,b,SD}\mathbf{\Lambda}_{\sqrt{P_0}}\mathbf{\Lambda}_{|\mathcal{H}_{SD}|^2}}{\mathbf{\Lambda}_{|\mathcal{H}_{SD}|^2} + \frac{\mathbf{\Lambda}_{\sigma^2_{\mathbf{V}_{SD}}}}{\mathbf{\Lambda}_{P_0}\mathbf{\Lambda}_{\sigma^2_{\mathbf{X}}}}} + \frac{\mathbf{\Lambda}_{\sqrt{P_1}}\mathbf{D}_{a,b,SRD}\mathbf{\Lambda}_{|\mathcal{H}_{RD}|^2}}{\mathbf{\Lambda}_{|\mathcal{H}_{RD}|^2} + \frac{\mathbf{\Lambda}_{\sigma^2_{\mathbf{V}_{RD}}}}{\mathbf{\Lambda}_{P_1}\mathbf{\Lambda}_{\sigma^2_{\mathbf{X}}}}} \right)\mathbf{X} + \\
&\quad \frac{\mathbf{D}_{a,b,SD}\mathcal{H}_{SD}^{\dagger}}{\mathbf{\Lambda}_{|\mathcal{H}_{SD}|^2} + \frac{\mathbf{\Lambda}_{\sigma^2_{\mathbf{V}_{SD}}}}{\mathbf{\Lambda}_{P_0}\mathbf{\Lambda}_{\sigma^2_{\mathbf{X}}}}}\mathbf{V}_{SD} + \mathbf{D}_{a,b,SRD}\left(\frac{\mathbf{\Lambda}_{\sqrt{P_1}}\mathbf{\Lambda}_{|\mathcal{H}_{RD}|^2}}{\mathbf{\Lambda}_{|\mathcal{H}_{RD}|^2} + \frac{\mathbf{\Lambda}_{\sigma^2_{\mathbf{V}_{RD}}}}{\mathbf{\Lambda}_{P_1}\mathbf{\Lambda}_{\sigma^2_{\mathbf{X}}}}}\mathbf{E} + \frac{\mathcal{H}_{RD}^{\dagger}}{\mathbf{\Lambda}_{|\mathcal{H}_{RD}|^2} + \frac{\mathbf{\Lambda}_{\sigma^2_{\mathbf{V}_{RD}}}}{\mathbf{\Lambda}_{P_1}\mathbf{\Lambda}_{\sigma^2_{\mathbf{X}}}}}\mathbf{V}_{RD} \right) \\
&= \mathbf{Z} + \mathbf{V}_{SRD}
\end{aligned}
\tag{3.43}
$$

$$
\begin{aligned}
\mathbf{\Lambda}_{\gamma_{a,DF}} &= \frac{\mathbb{E}\{\mathbf{Z}\mathbf{Z}^{\dagger}\}}{\mathbb{E}\{\mathbf{V}_{SRD}\mathbf{V}_{SRD}^{\dagger}\}} \\
&= \frac{\left(\frac{\mathbf{\Lambda}_{\sqrt{P_0}}\mathbf{D}_{a,b,SD}\mathbf{\Lambda}_{|\mathcal{H}_{SD}|^2}}{\mathbf{\Lambda}_{|\mathcal{H}_{SD}|^2} + \frac{\mathbf{\Lambda}_{\sigma^2_{\mathbf{V}_{SD}}}}{\mathbf{\Lambda}_{P_0}\mathbf{\Lambda}_{\sigma^2_{\mathbf{X}}}}} + \frac{\mathbf{\Lambda}_{\sqrt{P_1}}\mathbf{D}_{a,b,SRD}\mathbf{\Lambda}_{|\mathcal{H}_{RD}|^2}}{\mathbf{\Lambda}_{|\mathcal{H}_{RD}|^2} + \frac{\mathbf{\Lambda}_{\sigma^2_{\mathbf{V}_{RD}}}}{\mathbf{\Lambda}_{P_1}\mathbf{\Lambda}_{\sigma^2_{\mathbf{X}}}}} \right)^2 \mathbf{\Lambda}_{\sigma^2_{\mathbf{X}}}}{\frac{\mathbf{D}^2_{a,b,SD}\mathbf{\Lambda}_{|\mathcal{H}_{SD}|^2}}{\left(\mathbf{\Lambda}_{|\mathcal{H}_{SD}|^2} + \frac{\mathbf{\Lambda}_{\sigma^2_{\mathbf{V}_{SD}}}}{\mathbf{\Lambda}_{P_0}\mathbf{\Lambda}_{\sigma^2_{\mathbf{X}}}} \right)^2}\mathbf{\Lambda}_{\sigma^2_{\mathbf{V}_{SD}}} + \frac{\mathbf{\Lambda}_{P_1}\mathbf{D}^2_{a,b,SRD}\mathbf{\Lambda}_{|\mathcal{H}_{RD}|^4}}{\left(\mathbf{\Lambda}_{|\mathcal{H}_{RD}|^2} + \frac{\mathbf{\Lambda}_{\sigma^2_{\mathbf{V}_{RD}}}}{\mathbf{\Lambda}_{P_1}\mathbf{\Lambda}_{\sigma^2_{\mathbf{X}}}} \right)^2}\mathbf{\Lambda}_{\sigma^2_{\mathbf{E}}} + \frac{\mathbf{D}^2_{a,b,SRD}\mathbf{\Lambda}_{|\mathcal{H}_{RD}|^2}}{\left(\mathbf{\Lambda}_{|\mathcal{H}_{RD}|^2} + \frac{\mathbf{\Lambda}_{\sigma^2_{\mathbf{V}_{RD}}}}{\mathbf{\Lambda}_{P_1}\mathbf{\Lambda}_{\sigma^2_{\mathbf{X}}}} \right)^2}\mathbf{\Lambda}_{\sigma^2_{\mathbf{V}_{RD}}}},
\end{aligned}
\tag{3.44}
$$

respectively.

3.5 Summary

This chapter presented mathematical formulation about cooperative in-home PLC systems. The theoretical channel capacities and maximum data rates were obtained from the diagonal matrix of SNR for SD, SR and RD links, considering the AF and DF cooperative protocols and combining techniques such as EGC, SC and MRC.

4 MEASUREMENT CAMPAIGN

To experimentally analyze the benefits of a single relay model, a measurement campaign to acquire estimates of cooperative and in-home PLC channels was carried out in Brazil and details about such campaign are presented in the current chapter.

This chapter is organized as follows: Section 4.1 covers the equipment and measurement setup used and Section 4.2 discussed about some features of the PLC system as frequency response of links and PSD of additive noise.

4.1 Measurement Setup

For the characterization of such PLC channels, seven middle class residences in a typical urban area in the city of Juiz de Fora, Brazil, were considered. Some features of these places are listed in Table 1. More details about the residences are in Appendix B. These residences are representative of a large percentage of Brazilian residences. The used measurement setup is composed of two rugged personal computers equipped with data acquisition and generation boards connected to the power cable by a coupling circuit [33], as Fig. 8. The coupler is constituted by a high pass filter that blocks the main voltages (50 or 60 Hz) in order to avoid equipment damage. As it can be seen in Fig. 9, its frequency response is the most flat possible to not interfere in the system performance. With this equipment, it is constructed the setup of Figure 10. Firstly, the signal is generated in the waveform generation board (Tx) and injected into the power cable through the electrical outlet. On the other side of the electric power grids, the extracted signal is digitized by a data acquisition board (Rx).

Table 1: Main features of the measured places.

Construction type	Age (years)	Constructed area (m^2)
Residence #1	30	78
Residence #2	10	69
Residence #3	9	54
Residence #4	9	42
Residence #5	18	65
Residence #6	3	62
Residence #7	2	54

Also, a sounding-based method was applied to estimate the frequency response of the measured channels. This technique uses the knowledge of the generated and injected signal and its corresponding in the communication channel output [34]. As the focused scheme was the HS-OFDM, the output signal coefficients are real, suitable for data transmission in the baseband. The set of parameters used in the methodology to estimate the frequency response of in-home PLC channels is summarized in Table 2. In
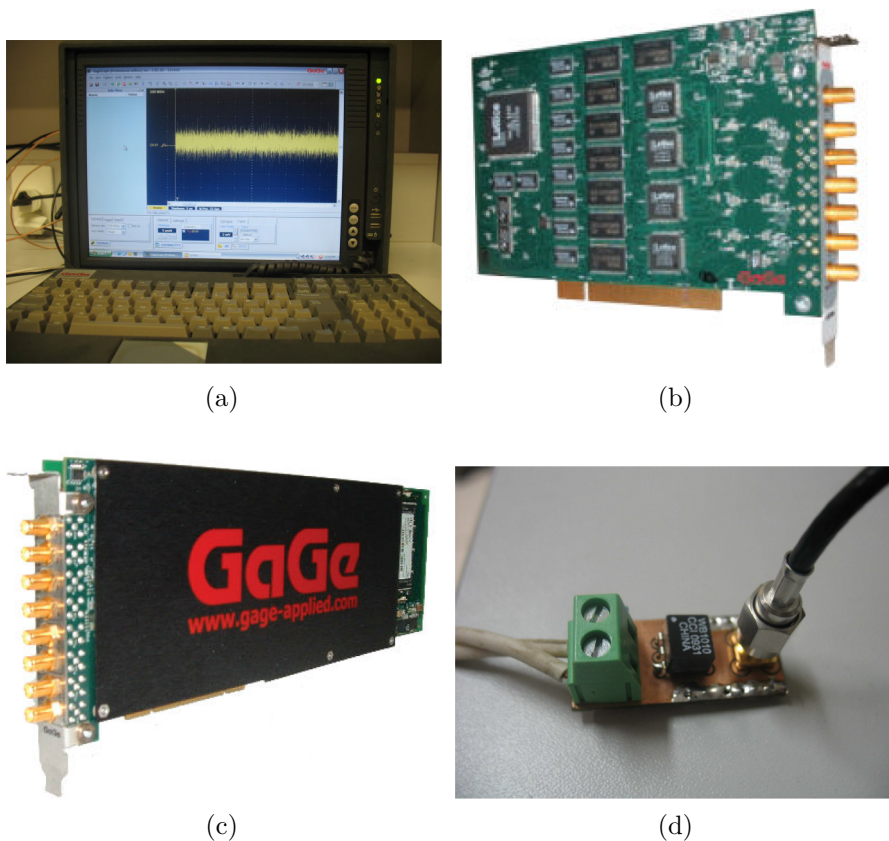
Figure 8: Equipment.

this measurement campaign, more than $36,000$ estimates of in-home PLC channels, whose physical electric circuits cover distances from 2 to 10 m, were obtained from the measured data and classified as SD, SR or RD links. The frequency band from 1.7 MHz up 100 MHz was covered.

Table 2: Main parameters adopted by the technique applied to estimate the PLC channel frequency responses.

Description	Value
Sampling frequency	$f_s = 200$ MHz
Number of sub-carriers	$N = 2048$
Modulation	BPSK
Cyclic prefix length	$L_{cp} = 512$
Frequency resolution	48.83 kHz
Symbol duration	23.04 μs

4.2   Measures of Cooperative and In-home PLC Channels

Figure 11 shows the adopted locations for the R node during the measurement campaign. Basically, the R node was located in the middle between the S and D nodes (case #1); near the D node (case #2); near the S node (case #3); and far from both S
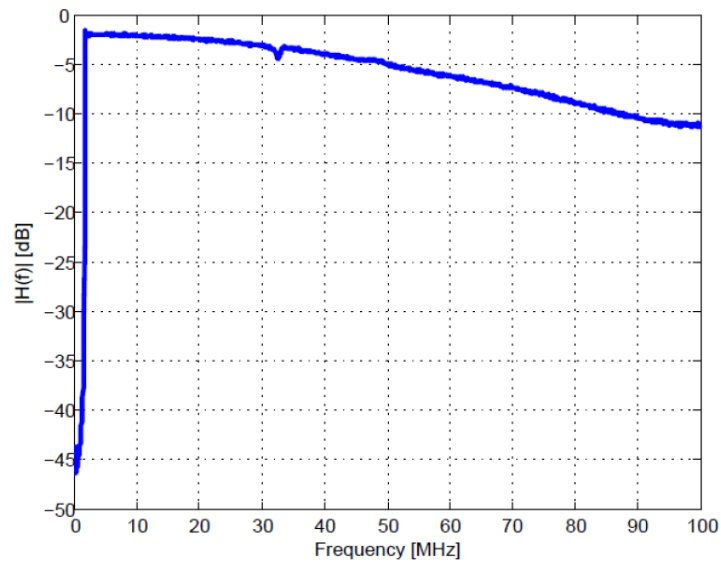
Figure 9: Coupler frequency response.
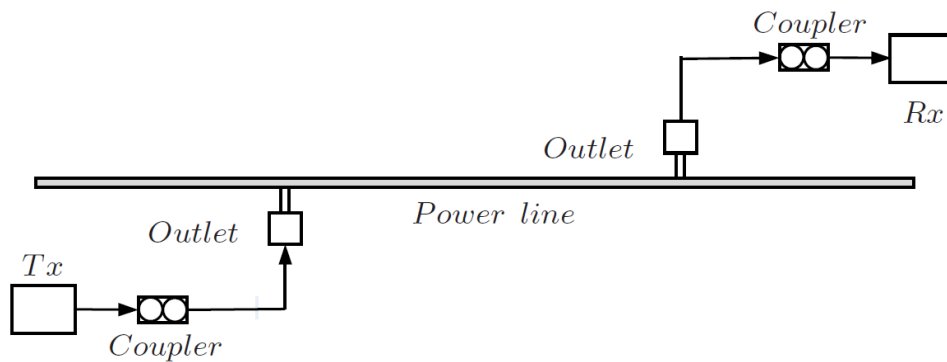
Figure 10: An example of the use of the measurement setup.

and D nodes (case #4). These cases cope with different settings that are found in a home, where the relay, the source and the destination nodes belong to the same electrical circuit. The analysis of these cases can reveal in which locations the R node can benefit in-home PLC systems.

Figure 12 shows the mean values of amplitude spectra of measured PLC channel frequency responses for SD, SR, RD, and SRD links for case #1, case #2, case #3 and case #4, respectively. Regarding case #1 (Fig. 12a), it can be seen that the attenuation profiles for SR and RD links are lower than that noted in the SD link (distances involving the SD link are longer), which is in accordance with the theory related to the wave propagation in a non-ideal conductor (attenuation increases with frequency and distance). A carefully analysis of this plot indicates that the use of the DF protocol at the R node may result in improved performance if the errored symbol detection probability at the R node tends to zero. On the other hand, the attenuation profiles of channel frequency responses for the SRD link show that attenuation is extremely high and, as a consequence, the AF protocol may not offer improvement. In the Chapter 5, this statement is validated
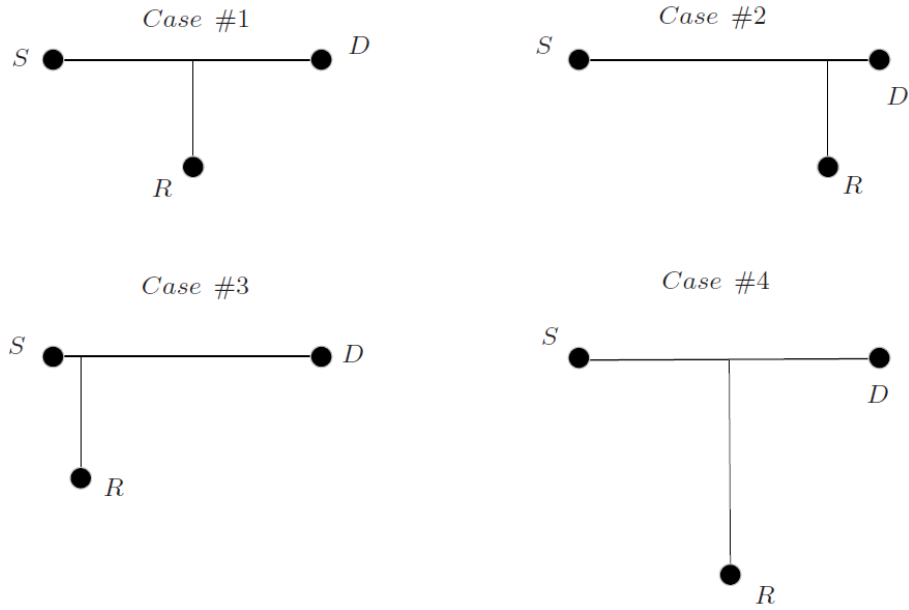
Figure 11: Relay locations based on electrical wiring distances.

with numerical results.

Following the same reasoning, in Figure 12b, it can be observed that the RD link has the lowest attenuation, as expected, since the R node is closest to the destination. On the other hand, in case #3, as the R node is near the source, then the SR link shows the lowest attenuation, see Figure 12c. Finally, in Figure 12d, there is a strong attenuation for SR, RD and SRD links. Thus, when the R node is away from the S and the D nodes, cooperation may not be advantageous.

Last, but not least, Figure 13 depicts estimates of the PSD of the measured additive noise for the SD, SR, and RD links, respectively, for cases #1, #2, #3 and #4. As expected, their profiles are almost the same. The reason for this is the fact that the electric circuit works as a bus, therefore, a significant change of the PSD of the noise, in the same electric circuit, is not expected. Due to the fact that the PSDs of SD and RD links refer to the additive noise at the D node measured during time slots #1 and #2, the mean value of the PSD of both SD and RD links is assumed for obtaining the numerical results.

4.3 Summary

This chapter presented in detail the measurement setup used through the figures of equipment and connection between it. In addition, frequency response and PSDs of measured additive noise were shown for the four cases.
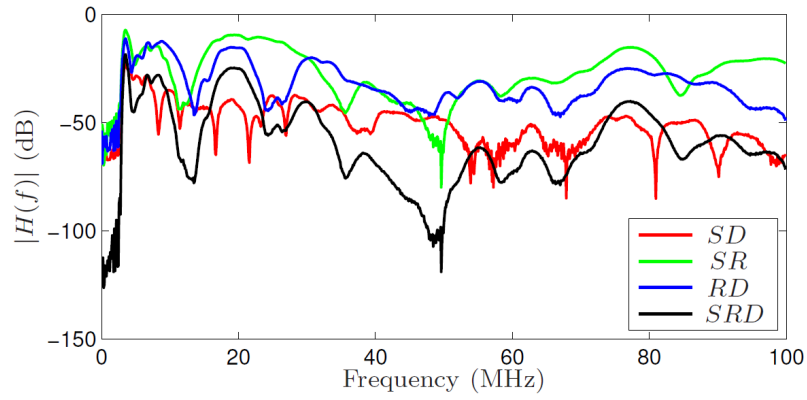
(a) case #1: midway.
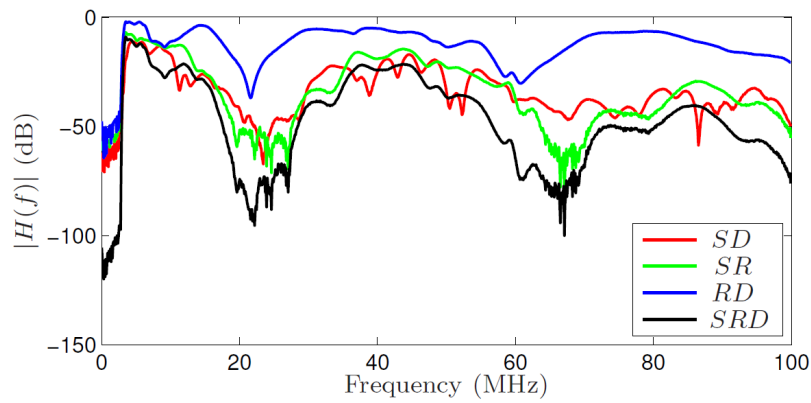
(b) case #2: near D node.
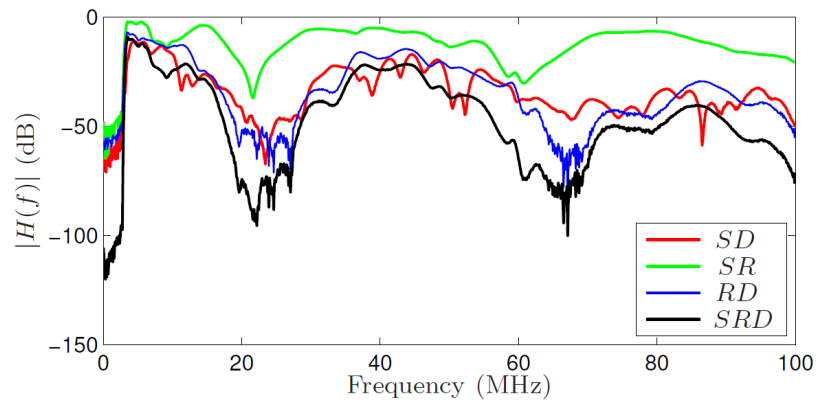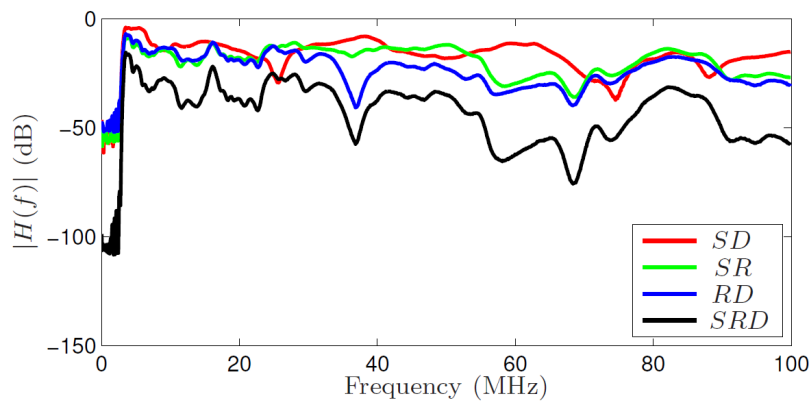
(c) case #3: near S node.

(d) case #4: far from S and D nodes.

Figure 12: Attenuation profiles of the frequency response of SD, SR, RD, and SRD links.
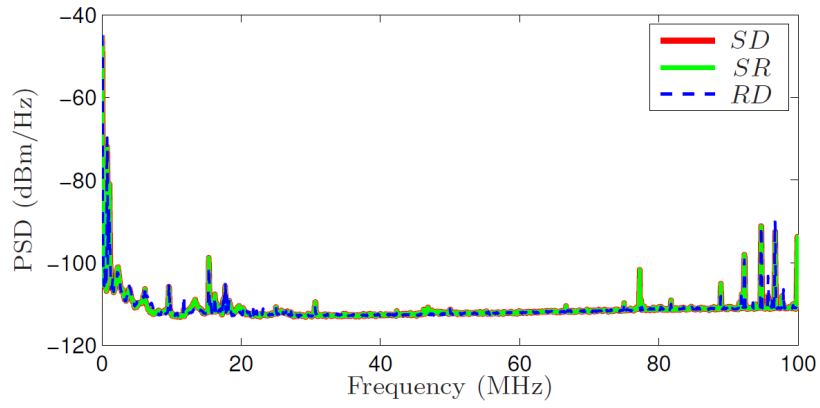
(a) case #1: midway.
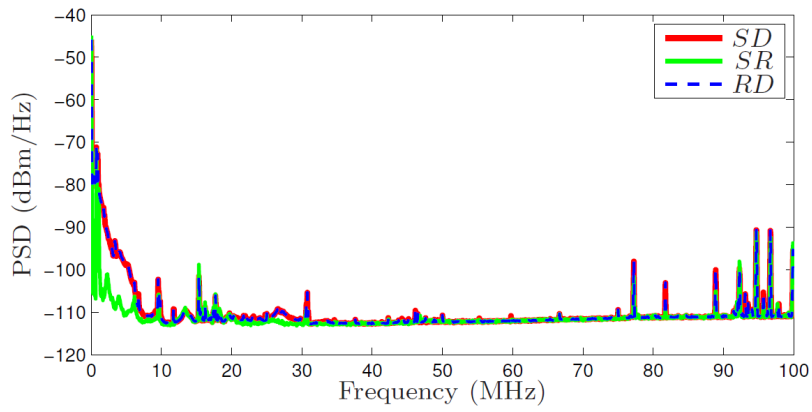
(b) case #2: near D node.
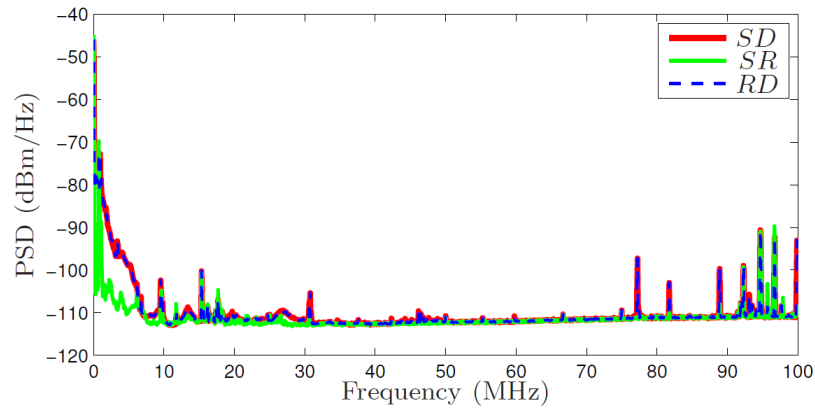
(c) case #3: near S node.
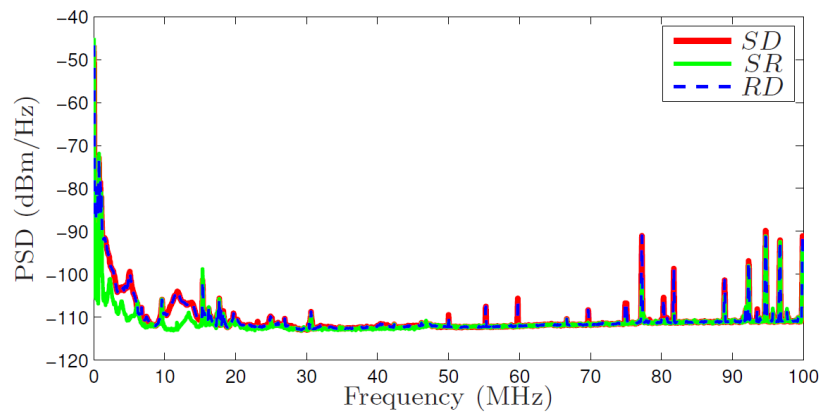
(d) case #4: far from S and D nodes.

Figure 13: PSD of measured additive noises in the SD, SR, and RD links.

5 NUMERICAL RESULTS

This chapter presents theoretical channel capacity and maximum data rate (HS-OFDM scheme) analyses of the measured cooperative and in-home PLC channels. All results are obtained when average gains of the channel frequency responses of the measured in-home PLC channels and PSDs for SD, SR, RD and SRD links in the four cases are considered. This choice offers a good picture of what kind of performance, on average, can be expected by applying cooperative protocol at the physical layer and analyses are based on measured data.

By considering a measured data set consisting of in-home PLC channels and additive noises, analyses based on numerical results for three different frequency bands: 1.7-30 MHz, 1.7-50 MHz and 1.7-100 MHz are presented and represented as B_{30}, B_{50} and B_{100}, respectively. The first and the second frequency bands comply with European and Brazilian regulations for PLC systems, respectively, while the latter is a possibility for future regulation and standardization. The values of theoretical channel capacities are evaluated according to Chapter 3 as well as the value of maximum data rates obtained by the use of HS-OFDM together with the cooperative protocols and combining techniques.

The remainder of this chapter is organized as follows: Section 5.1 discusses the attained results when the total power is optimally allocated to all subcarriers and the CSI is available at the transmitter and Section 5.2 shows the normalized channel capacity and maximum data rate when CSI is not available at the transmitter and the total power is uniformly allocated to all subcarriers. In all these analyses, it is assumed $\mathbf{E} = \mathbf{0}$ (the relay correctly detects the received symbols). On the other hand, Section 5.3 numerically evaluates the cooperative and in-home PLC system performance when $\mathbf{E} \neq \mathbf{0}$.

5.1 Optimal Total Power Allocation (OA)

In order to verify the influence of total power and frequency bandwidth on the performance of cooperative and in-home PLC systems, the theoretical channel capacity was evaluated when $P \in \{-20, -10, 0, 10, 20, 30\}$ dBm and the choice of P_0 and P_1 and their distribution among the subcarriers are those that maximize the mutual information between the transmitted and received signals and are obtained using the water-filling algorithm. Tables 3-6 list the normalized theoretical channel capacity for the AF and DF protocols for each case where

$$\bar{C}_\beta = \frac{C_\beta}{C_{\max}}, \tag{5.1}$$

in which $\beta \in \{\text{AF,DF}\}$ and $C_{\max} = \max_{P_0} C_{SD}$ subject to $P_0 + P_1 \leq P$ is the theoretical channel capacity associated with the SD link. These tables show that the DF protocol can

Table 3: Normalized theoretical channel capacities $\bar{C}_\beta$ for case #1 and OA.

P (dBm)	AF			DF		
	B_{30}	B_{50}	B_{100}	B_{30}	B_{50}	B_{100}
-20	1.00	1.00	1.00	2.07	2.59	3.98
-10	1.00	1.00	1.00	1.68	1.98	2.92
0	1.00	1.00	1.00	1.48	1.66	2.28
10	1.06	1.03	1.01	1.37	1.50	1.87
20	1.18	1.12	1.06	1.30	1.39	1.63
30	1.35	1.30	1.16	1.26	1.33	1.49

Table 4: Normalized theoretical channel capacities $\bar{C}_\beta$ for case #2 and OA.

P (dBm)	AF			DF		
	B_{30}	B_{50}	B_{100}	B_{30}	B_{50}	B_{100}
-20	1.00	1.00	1.00	1.18	1.28	1.44
-10	1.00	1.00	1.00	1.14	1.21	1.32
0	1.01	1.00	1.00	1.11	1.16	1.24
10	1.12	1.06	1.02	1.10	1.13	1.19
20	1.29	1.19	1.09	1.08	1.11	1.15
30	1.46	1.36	1.22	1.07	1.10	1.13

Table 5: Normalized theoretical channel capacities $\bar{C}_\beta$ for case #3 and OA.

P (dBm)	AF			DF		
	B_{30}	B_{50}	B_{100}	B_{30}	B_{50}	B_{100}
-20	1.00	1.00	1.00	1.07	1.02	1.13
-10	1.00	1.00	1.00	1.05	1.01	1.08
0	1.01	1.00	1.00	1.05	1.01	1.06
10	1.12	1.06	1.02	1.04	1.01	1.05
20	1.29	1.19	1.09	1.04	1.01	1.04
30	1.46	1.36	1.22	1.03	1.01	1.03

improve the PLC system performance if zero symbol error probability is assumed at the R node. These improvements can be observed in case #1, case #2 and case #3 for $P \leq 30$ dBm. Moreover, the case #1 is the situation in which the improvement is more evident, for any value of P. Furthermore, these tables emphasize that cooperative communication through the DF protocol increasingly improves in-home PLC system performance if P decreases and/or the frequency range increases. It is worth noting that the AF protocol offers improvements in all cases, although these are more significant if P increases and/or the frequency range decreases. Last, but not least, the frequency band from 1.7 up to 100 MHz offers the best results when the DF protocol is considered. On the other hand, for the AF protocol, the highest normalized theoretical capacities occur when the frequency band is from 1.7 up to 30 MHz because the attenuation profile in the SRD link is the lowest in comparison with other frequency bands. In other words, the attenuation associated with the increase of frequency bandwidth severely degrade AF protocol.

Table 6: Normalized theoretical channel capacities $\bar{C}_\beta$ for case #4 and OA.

P (dBm)	AF			DF		
	B_{30}	B_{50}	B_{100}	B_{30}	B_{50}	B_{100}
-20	1.00	1.00	1.00	0.85	0.78	0.73
-10	1.00	1.00	1.00	0.87	0.82	0.78
0	1.01	1.00	1.00	0.89	0.85	0.82
10	1.07	1.04	1.01	0.90	0.87	0.85
20	1.18	1.10	1.04	0.92	0.88	0.87
30	1.31	1.19	1.09	0.92	0.90	0.88

A normalized maximum data rate comparison was carried out when the HS-OFDM scheme with FDE-ZF and FDE-MMSE and in-home PLC channel corrupted by additive colored Gaussian noises are considered and evaluated by (5.1). In this situation, $\beta \in \{SD,AF\text{-}SRD,DF\text{-}SRD,AF\text{-}EGC,DF\text{-}EGC,AF\text{-}SC,DF\text{-}SC,AF\text{-}MRC,DF\text{-}MRC\}$, $C_{\max} = \max_{P_0} C_{SD}$ subject to $P_0 + P_1 \leq P$ is the maximum data rate associated with SD link and C_β is the maximum data rate related to the β link for a given total power.

The attained values for the normalized maximum data rates are presented in Tables 7-10, by assuming $P = 20$ dBm, P_0 and P_1 optimally allocated at the subcarriers. In these tables, AF-EGC, DF-EGC, AF-SC, DF-SC, AF-MRC and DF-MRC denote the protocol and the combining technique used in each analysis; FDE-ZF and FDE-MMSE refer to the HS-OFDM scheme associated with use of FDE based on the ZF and MMSE criteria, respectively. By representing a new frequency band under study for PLC systems, the frequency band 1.7-100 MHz was utilized to evaluate the normalized maximum data rates for the AF and DF protocols. As previously discussed, the DF protocol can improve the performance of HS-OFDM scheme if case #1, case #2 and case #3 are considered. Additionally, the MRC protocol results in the best performance and the EGC in the worst one. Due to the small difference observed between the performance attained by the MRC and SC, a choice in favor of SC is reasonable because it demands lower hardware complexity than the MRC. This improvement can be confirmed by analyzing Table 7 (case #1) together with the plot in Figure 15b when, for instance, $P = 20$ dBm. As we can see, the use of the HS-OFDM scheme together with FDE-MMSE achieves $C_{SD} = 428.7$ Mbps, the maximum data rate of SD link and $C_{DF-MRC} = 749.6$ Mbps is the maximum data rate when the DF protocol, MRC technique and optimal power allocation (OA) are considered, resulting in $\bar{C}_{DF-MRC} = 1.75$. For other cases these values are: $C_{SD} = 709.2$ Mbps, $C_{DF-MRC} = 795$ and $\bar{C}_{DF-MRC} = 1.12$ (case #2); $C_{SD} = 709.2$ Mbps, $C_{DF-MRC} = 758$ and $\bar{C}_{DF-MRC} = 1.07$ (case #3); $C_{SD} = 488.4$ Mbps, $C_{DF-MRC} = 489.9$ and $\bar{C}_{DF-MRC} = 1.00$ (case #4), it can be seen in Tables 8-10, respectively. Regarding the adopted criterion in the FDE, we noted that the FDE-MMSE attains almost the same performance of FDE-ZF.

Table 7: Normalized maximum data rates $\bar{C}_\beta$ for case #1, considering $P = 20$ dBm, B_{100} and OA.

	AF		DF	
	FDE-ZF	FDE-MMSE	FDE-ZF	FDE-MMSE
SD	1.00	1.00	1.00	1.00
SRD	0.06	0.06	1.75	1.75
EGC	0.69	1.00	1.09	1.11
SC	1.00	1.00	1.75	1.75
MRC	1.00	1.00	1.75	1.75

Table 8: Normalized maximum data rates $\bar{C}_\beta$ for case #2, considering $P = 20$ dBm, B_{100} and OA.

	AF		DF	
	FDE-ZF	FDE-MMSE	FDE-ZF	FDE-MMSE
SD	1.00	1.00	1.00	1.00
SRD	0.09	0.09	1.05	1.05
EGC	0.70	0.99	1.03	1.03
SC	1.00	1.00	1.07	1.07
MRC	1.00	1.00	1.12	1.12

Table 9: Normalized maximum data rate $\bar{C}_\beta$ for case #3, considering $P = 20$ dBm, B_{100} and OA.

	AF		DF	
	FDE-ZF	FDE-MMSE	FDE-ZF	FDE-MMSE
SD	1.00	1.00	1.00	1.00
SRD	0.09	0.09	1.05	1.05
EGC	0.70	0.99	0.98	0.98
SC	1.00	1.00	1.05	1.05
MRC	1.00	1.00	1.07	1.07

Table 10: Normalized maximum data rate $\bar{C}_\beta$ for case #4, considering $P = 20$ dBm, B_{100} and OA.

	AF		DF	
	FDE-ZF	FDE-MMSE	FDE-ZF	FDE-MMSE
SD	1.00	1.00	1.00	1.00
SRD	0.04	0.04	0.76	0.76
EGC	0.35	0.98	0.82	0.82
SC	1.00	1.00	0.99	0.99
MRC	1.00	1.00	1.00	1.00

Table 11: Normalized theoretical channel capacities $\bar{C}_\beta$ for case #1 and UA.

P (dBm)	AF			DF		
	B_{30}	B_{50}	B_{100}	B_{30}	B_{50}	B_{100}
-20	1.00	1.00	1.00	2.11	2.74	5.30
-10	1.00	1.00	1.00	1.69	2.00	3.25
0	1.00	1.00	1.00	1.49	1.67	2.34
10	1.03	1.01	1.00	1.38	1.50	1.88
20	1.16	1.09	1.03	1.31	1.40	1.63
30	1.34	1.29	1.13	1.26	1.33	1.49

Table 12: Normalized theoretical channel capacities $\bar{C}_\beta$ for case #2 and UA.

P (dBm)	AF			DF		
	B_{30}	B_{50}	B_{100}	B_{30}	B_{50}	B_{100}
-20	1.00	1.00	1.00	1.21	1.30	1.46
-10	1.00	1.00	1.00	1.16	1.22	1.32
0	1.00	1.00	1.00	1.13	1.17	1.24
10	1.09	1.04	1.00	1.11	1.14	1.19
20	1.30	1.18	1.07	1.10	1.12	1.15
30	1.50	1.38	1.21	1.09	1.10	1.13

Table 13: Normalized theoretical channel capacities $\bar{C}_\beta$ for case #3 and UA.

P (dBm)	AF			DF		
	B_{30}	B_{50}	B_{100}	B_{30}	B_{50}	B_{100}
-20	1.00	1.00	1.00	1.14	1.08	1.05
-10	1.00	1.00	1.00	1.10	1.06	1.02
0	1.00	1.00	1.00	1.08	1.04	1.00
10	1.09	1.04	1.04	1.07	1.04	1.00
20	1.30	1.18	1.17	1.06	1.03	1.00
30	1.50	1.38	1.35	1.05	1.03	1.00

5.2   Uniform Power Allocation (UA)

When the CSI is not available at the transmitter, the uniform power allocation (UA) is the most recommended strategy to perform power allocation in the subcarriers. To verify the influence of total power and frequency bandwidth on the performance of cooperative protocol on the in-home PLC system under this situation (lack of CSI at the transmitter), the theoretical channel capacity was evaluated when $P \in \{-20, -10, 0, 10, 20, 30\}$ dBm. Tables 11-14 list the normalized theoretical channel capacity for the case #1 when (5.1) and cooperative protocols are considered, in which $\beta \in \{\text{AF}, \text{DF}\}$ and $C_{\max} = \max_{P_0} C_{SD}$ subject to $P_0 + P_1 \leq P$. This table shows the DF protocol advantage over the AF protocol occurs, mainly when P decreases and the bandwidth increases. Furthermore, the highest normalized theoretical channel capacities occur in the 1.7-30 MHz frequency band for the AF protocol and in the 1.7-100 MHz frequency band for the DF protocol.

Table 14: Normalized theoretical channel capacities $\bar{C}_\beta$ for case #4 and UA.

	AF			DF		
P (dBm)	B_{30}	B_{50}	B_{100}	B_{30}	B_{50}	B_{100}
-20	1.00	1.00	1.00	1.03	1.05	1.46
-10	1.00	1.00	1.00	1.02	1.04	0.72
0	1.00	1.00	1.00	1.02	1.04	0.78
10	1.03	1.04	1.00	1.01	1.04	0.82
20	1.19	1.10	1.03	1.01	1.02	0.85
30	1.37	1.25	1.08	1.00	1.02	0.88

Table 15: Normalized maximum data rate $\bar{C}_\beta$ for case #1, considering $P = 20$ dBm, B_{100} and UA.

	AF		DF	
	FDE-ZF	FDE-MMSE	FDE-ZF	FDE-MMSE
SD	1.00	1.00	1.00	1.00
SRD	0.06	0.06	1.75	1.75
EGC	0.68	1.00	1.09	1.10
SC	1.00	1.00	1.75	1.75
MRC	1.00	1.00	1.75	1.75

Table 16: Normalized maximum data rate $\bar{C}_\beta$ for case #2, considering $P = 20$ dBm, B_{100} and UA.

	AF		DF	
	FDE-ZF	FDE-MMSE	FDE-ZF	FDE-MMSE
SD	1.00	1.00	1.00	1.00
SRD	0.09	0.09	1.05	1.05
EGC	0.70	0.99	1.03	1.03
SC	1.00	1.00	1.07	1.07
MRC	1.00	1.00	1.12	1.12

The attained values for the normalized maximum data rates are presented in Tables 15-18, by assuming $P = 20$ dBm and P_0 and P_1 uniformly allocated at subcarriers. As previously discussed, the DF protocol is more beneficial for cases #1, #2 and #3, mainly if P decreases. This improvement is observed through Table 15 (case #1) and the plot in Figure 15b when, for instance, $P = 20$ dBm. In this situation, $C_{SD} = 427.7$ Mbps and $C_{DF-MRC} = 749.5$ Mbps are the maximum data rate for SD link and DF-MRC technique, respectively, resulting in $\bar{C}_{DF-MRC} = 1.75$ when UA is considered. The MRC combining technique results in the best result and the EGC in the worst one and there is a small difference between the performance attained by the MRC and SC techniques.

Looking at the plots of Figures 14-21, it is clear that if the OA is adopted, the AF protocol can provide gains when the total power increases and/or the frequency band decreases (cases #1, #2 and #3). On the other hand, the DF protocol always provides gain which decreases as the frequency band decreases and/or the total power increases

Table 17: Normalized maximum data rate $\bar{C}_\beta$ for case #3, considering $P = 20$ dBm, B_{100} and UA.

	AF		DF	
	FDE-ZF	FDE-MMSE	FDE-ZF	FDE-MMSE
SD	1,00	1,00	1,00	1,00
SRD	0,09	0,09	1,05	1,05
EGC	0,70	0,99	0,98	0,98
SC	1,00	1,00	1,05	1,05
MRC	1,00	1,00	1,07	1,07

Table 18: Normalized maximum data rate $\bar{C}_\beta$ for case #4, considering $P = 20$ dBm, B_{100} and UA.

	AF		DF	
	FDE-ZF	FDE-MMSE	FDE-ZF	FDE-MMSE
SD	1.00	1.00	1.00	1.00
SRD	0.04	0.04	0.76	0.76
EGC	0.35	0.98	0.82	0.82
SC	1.00	1.00	0.99	0.99
MRC	1.00	1.00	1.00	1.00

(cases #1, #2 and #3). In case #4, the DF protocol does not improve performance, since in this scenario, the R node is very distant from the S and D nodes. Regarding the UA, it has similar behavior for both protocols, although the gains obtained by the AF protocol are the lowest or nonexistent.

5.3 Data Rate Degradation due to $\mathbf{E} \neq \mathbf{0}$

In order to evaluate the cooperative and in-home PLC system performance when $\mathbf{E} \neq \mathbf{0}$, it is presented the maximum data rates for all cases when HS-OFDM scheme, FDE with MMSE, MRC, $P = 20$ dBm are considered and the transmission power is optimally allocated by using the water-filling algorithm. Also, it is assumed that $\mathbf{E}$ is modeled as circular complex Gaussian such that $\mathbb{E}\{\mathbf{E}\} = \mathbf{0}$ and $\mathbb{E}\{\mathbf{E}\mathbf{E}^\dagger\} = \mathbf{\Lambda}_{\sigma_\mathbf{E}^2}$. It is introduced the parameter k which, although not having physical meaning, it assists the visualization of maximum data rate behavior when $\mathbf{E} \neq \mathbf{0}$. The value of k is given by $k = 10 \times \log_{10}\left[\dfrac{\text{Tr}\left(\mathbf{\Lambda}_{P_1}\mathbf{\Lambda}_{|\mathcal{H}_{RD}|^2}\mathbf{\Lambda}_{\sigma_\mathbf{E}^2}\right)}{\text{Tr}\left(\mathbf{\Lambda}_{\sigma_{\mathbf{V}_{RD}}^2}\right)}\right]$, which is formed from the relationship between the variances related to the error symbol detection and noise of RD link, see (3.32) and (3.44). Figures 22 and 23 show the degradation as k increases for all cases. In this scenario, $\mathbf{E}$ is assumed constant and the noise of RD link is varied. To better represent the plots of figures, the maximum data rate was normalized by the following factors: 5 Mbps (case #1), 8.75 Mbps (cases #2 and #3) and 5.6 Mbps (case #4). In general, it can observed that the FDE-MMSE is more robust than the FDE-ZF when the error symbol detection at
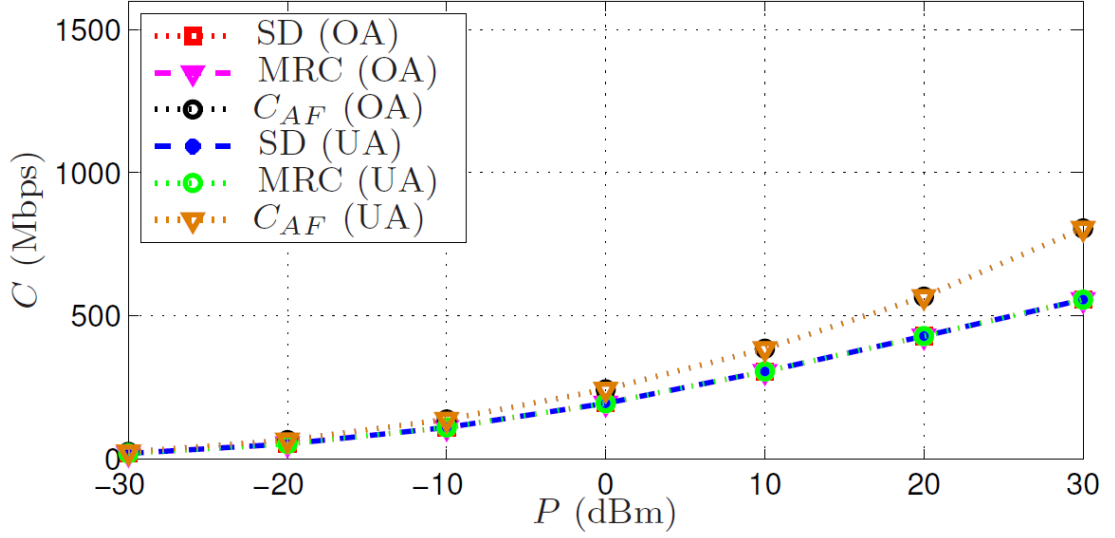
(a) FDE-ZF
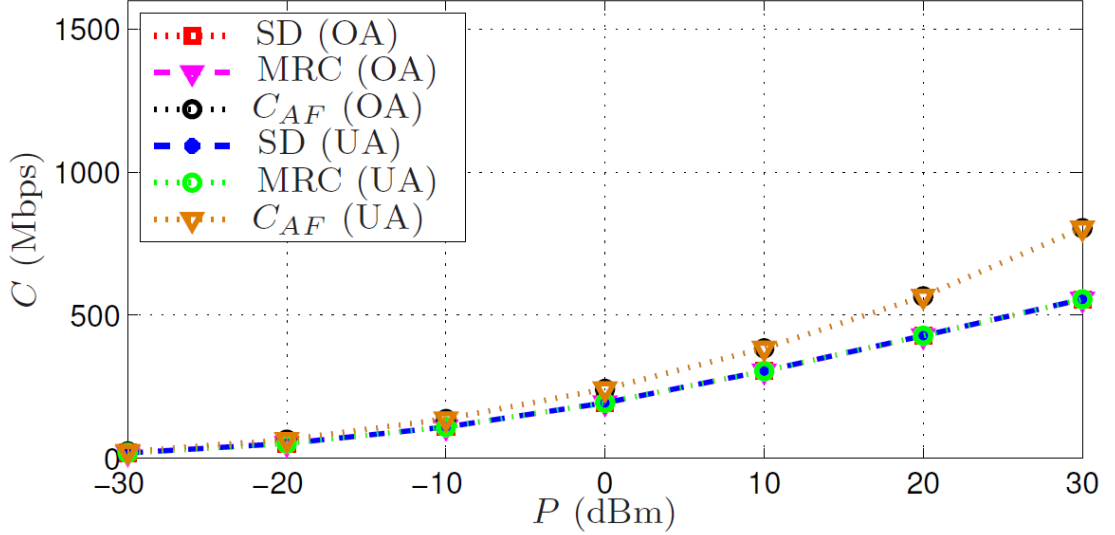
(b) FDE-MMSE

Figure 14: Maximum data rates and theoretical channel capacities for case #1 and B_{100}, using AF protocol and HS-OFDM scheme.

the relay node increases. It can be observed that, as k increases, the maximum data rate related to the DF protocol decreases. In Figure 22a, it can be noted that the DF protocol is not advantageous for $k \geq 40$ dB and $k \geq 30$ dB when FDE-MMSE and FDE-ZF are, respectively, considered for case #1. On the other hand, Figure 22b shows that for $k > 60$ dB (FDE-MMSE) and $k \geq 48$ dB (FDE-ZF), the DF protocol is not better than the AF one for case #2. For case #3 (Figure 23a, when $k > 60$ dB (FDE-MMSE) and $k \geq 38$ dB (FDE-ZF) there is not advantage in using the DF protocol. Finally, for case #4 (Figure 23b, both protocols show similar performances. The rationale for high values of k is the fact that the symbol error detection variance is multiplied by the gain of the PLC channel in the RD link as well as the amplification matrix ($\mathbf{\Lambda}_{P_1}$) at the R node.

(a) FDE-ZF

(b) FDE-MMSE
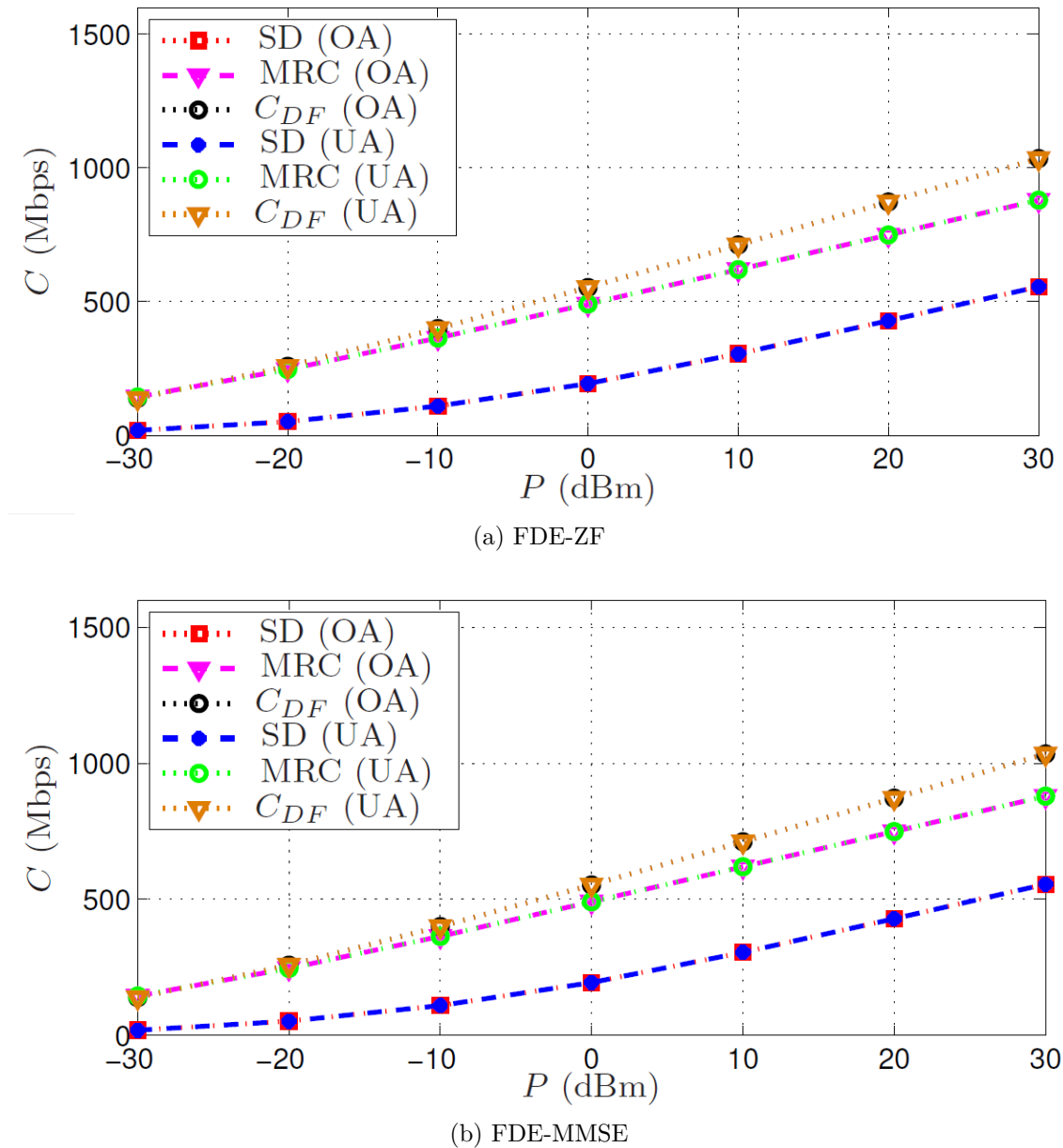
Figure 15: Maximum data rates and theoretical channel capacities for case #1 and B_{100}, using DF protocol and HS-OFDM scheme.

5.4   Summary

This chapter presented in detail the numerical results about theoretical channel capacity and maximum data rate of cooperative in-home PLC systems when the transmitted power is optimally and uniformly allocated. The influence of symbol detection errors at the R node in the DF protocol performance was also considered.
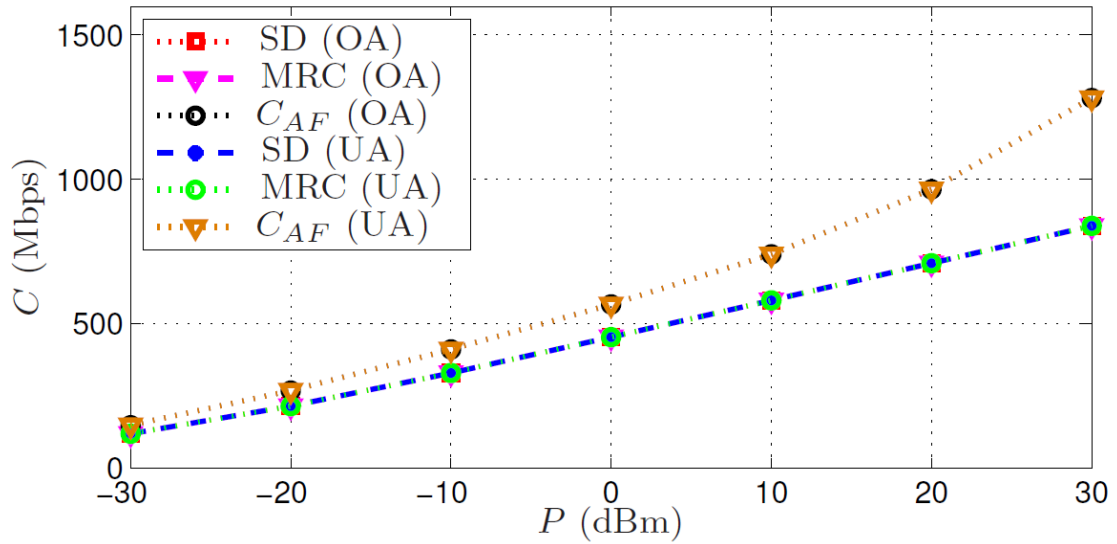
(a) FDE-ZF
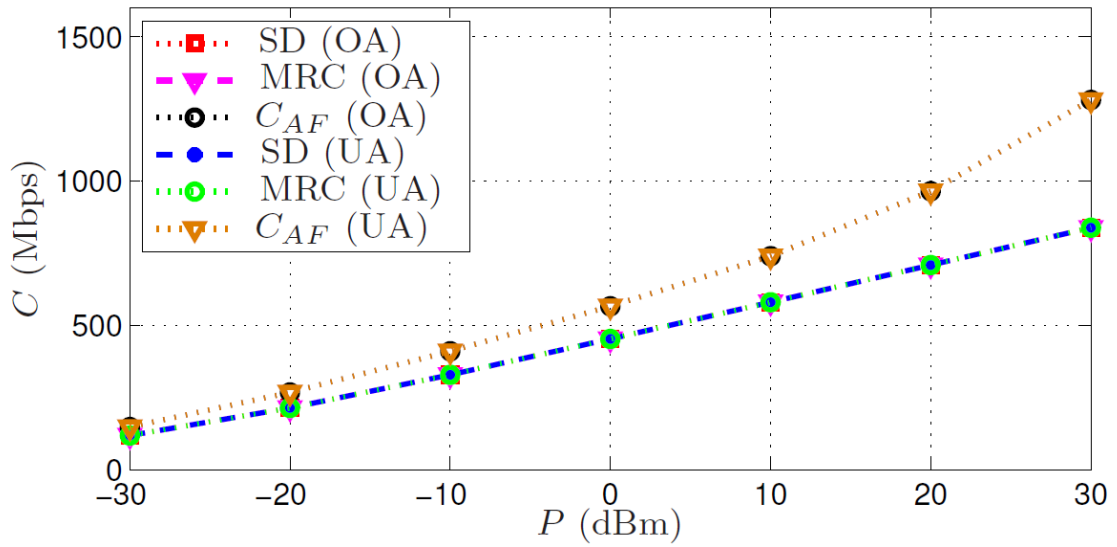
(b) FDE-MMSE

Figure 16: Maximum data rates and theoretical channel capacities for case #2 and B_{100}, using AF protocol and HS-OFDM scheme.
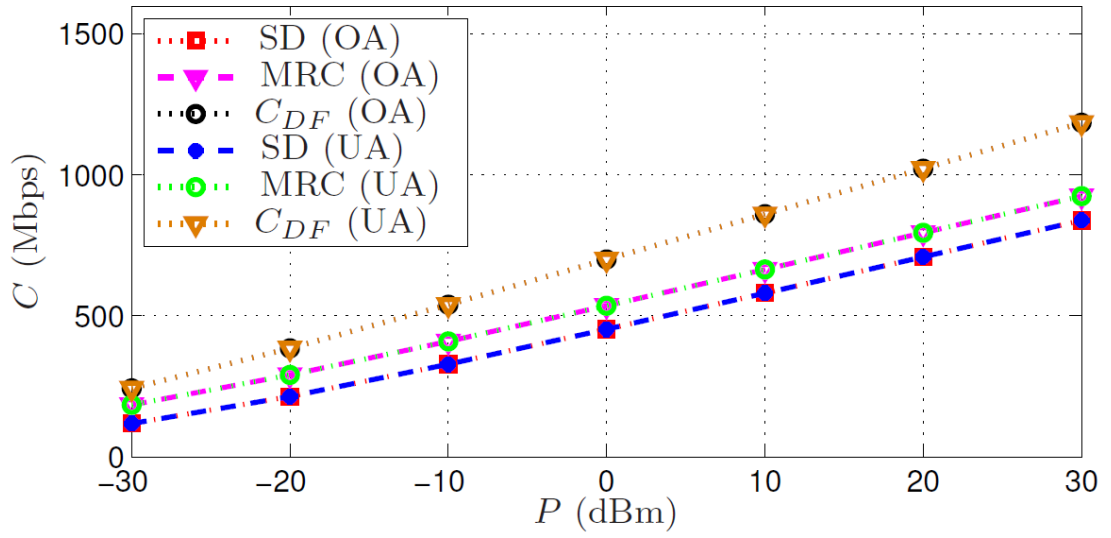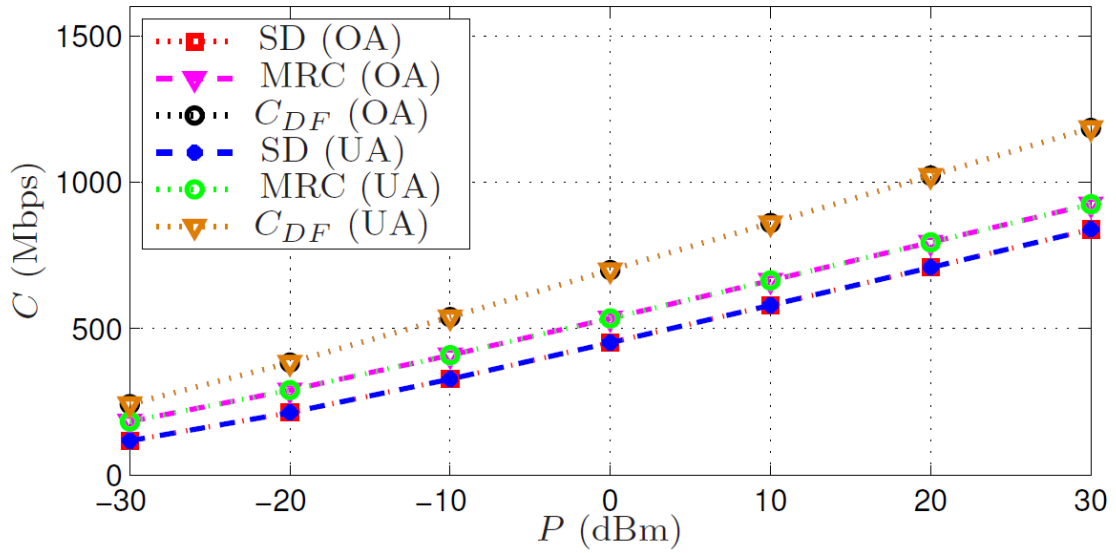
(a) FDE-ZF

(b) FDE-MMSE

Figure 17: Maximum data rates and theoretical channel capacities for case #2 and B_{100}, using DF protocol and HS-OFDM scheme.
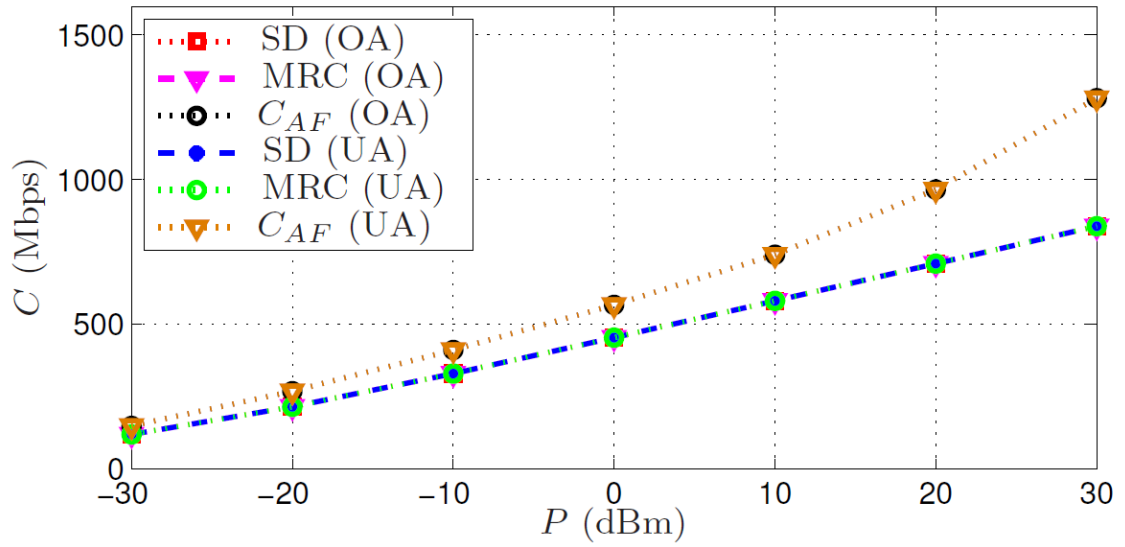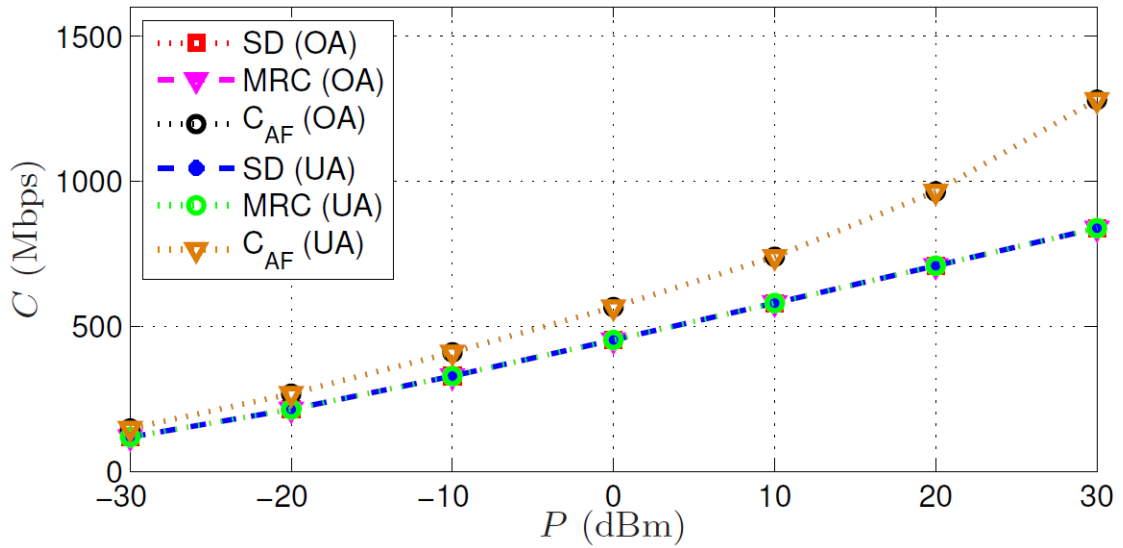
(a) FDE-ZF

(b) FDE-MMSE

Figure 18: Maximum data rates and theoretical channel capacities for case #3 and B_{100}, using AF protocol and HS-OFDM scheme.
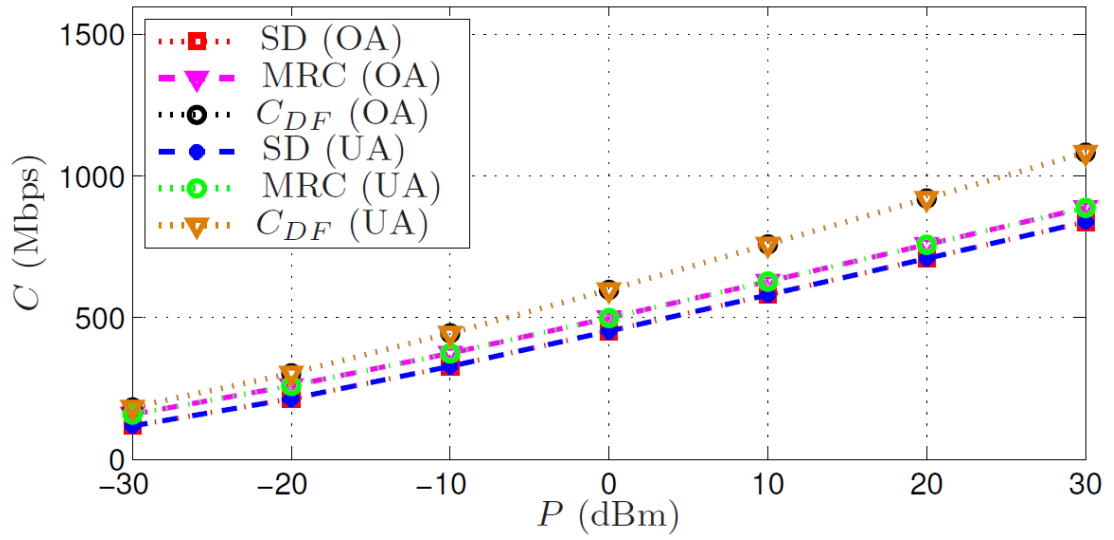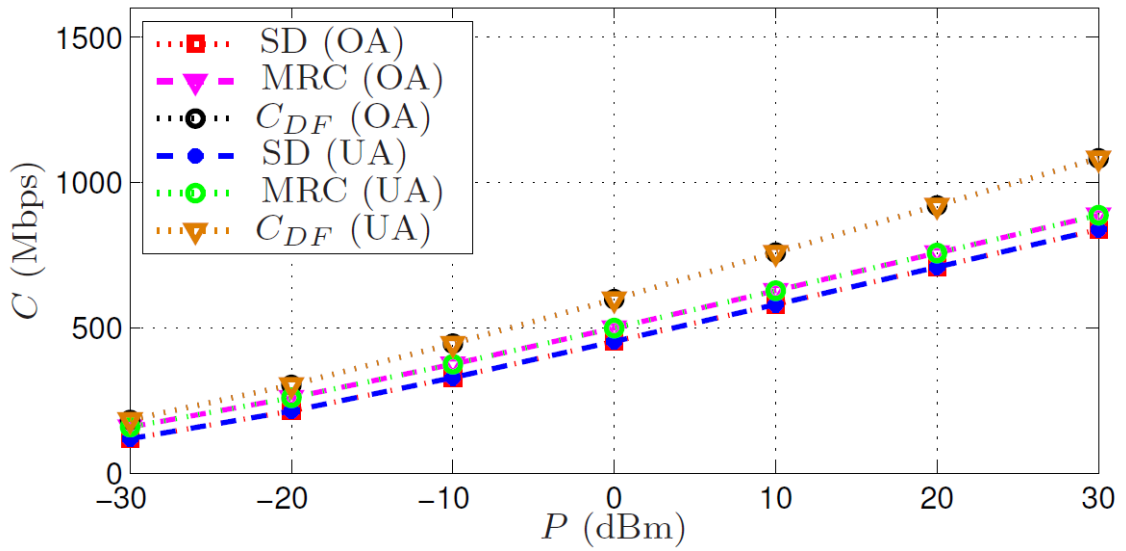
(a) FDE-ZF

(b) FDE-MMSE

Figure 19: Maximum data rates and theoretical channel capacities for case #3 and B_{100}, using DF protocol and HS-OFDM scheme.
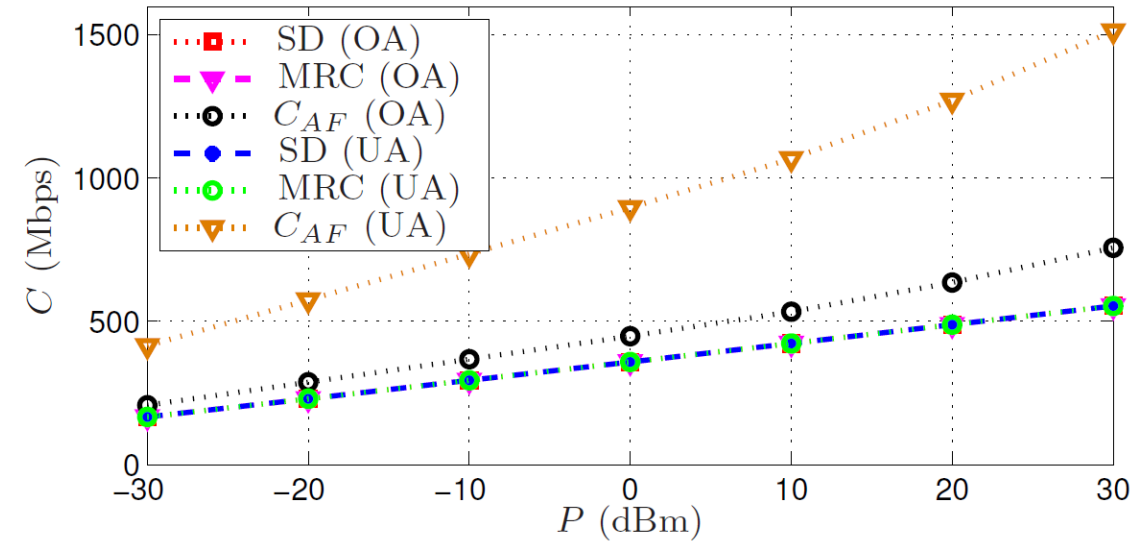
(a) FDE-ZF
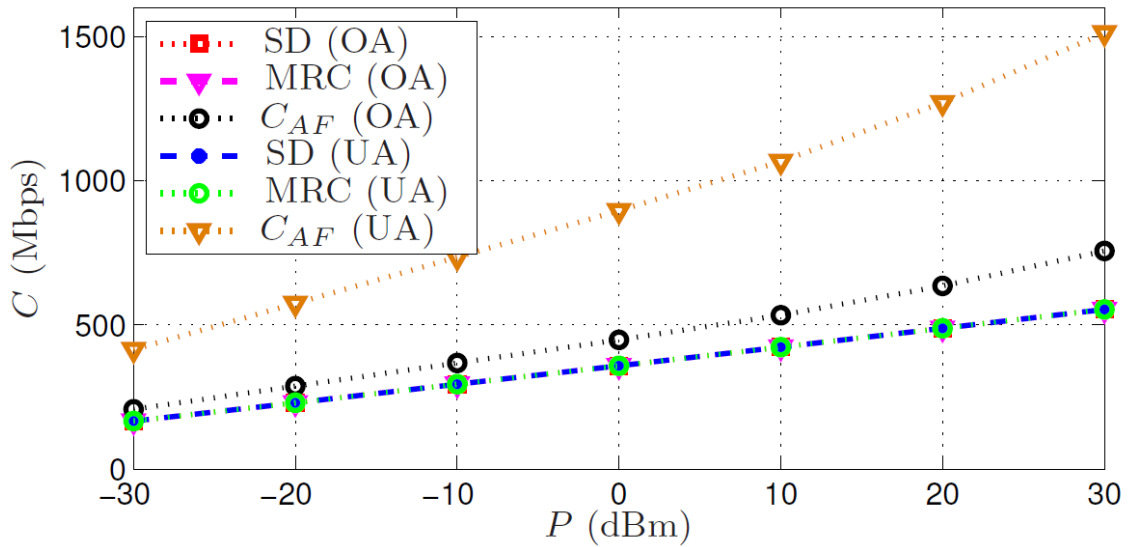
(b) FDE-MMSE

Figure 20: Maximum data rates and theoretical channel capacities for case #4 and B_{100}, using AF protocol and HS-OFDM scheme.

(a) FDE-ZF

(b) FDE-MMSE
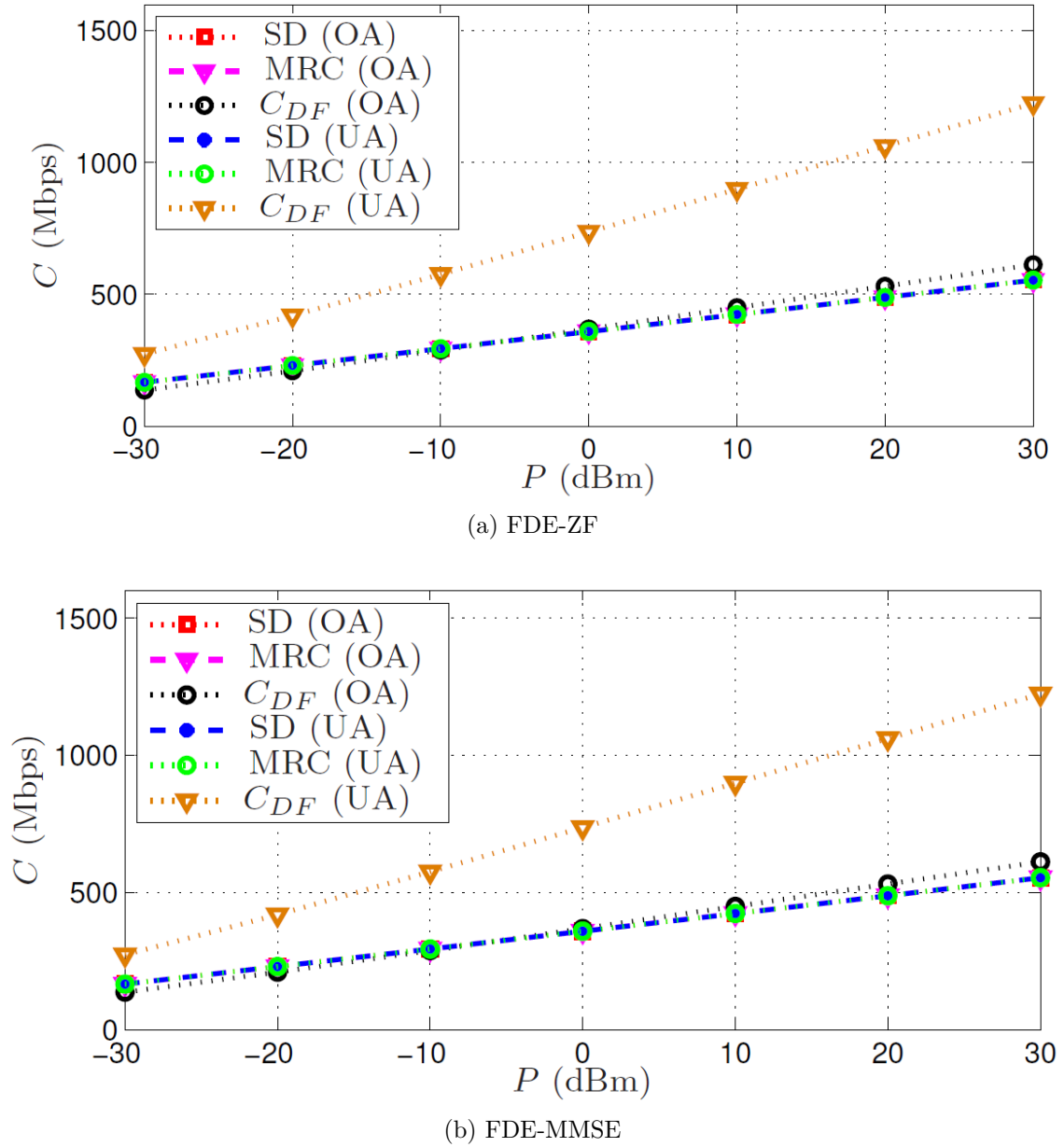
Figure 21: Maximum data rates and theoretical channel capacities for case #4 and B_{100}, using DF protocol and HS-OFDM scheme.
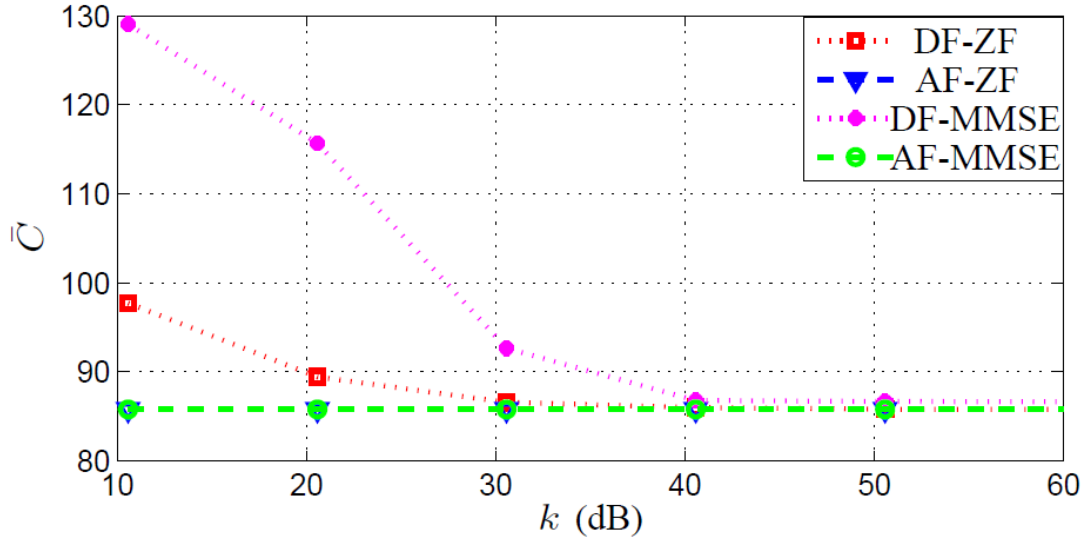
(a) case #1
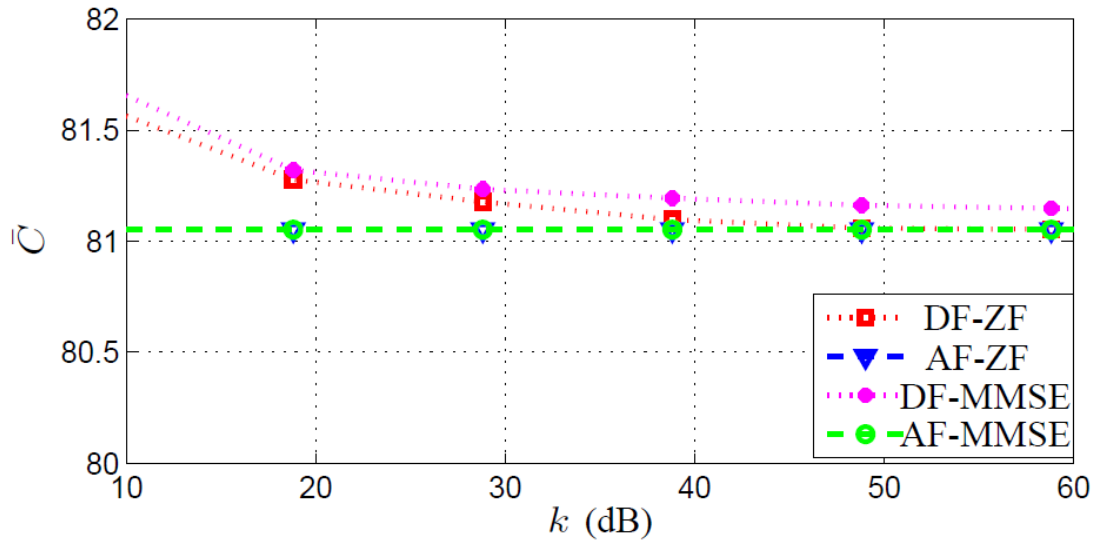
(b) case #2

Figure 22: Maximum data rates when $\mathbf{E} \neq \mathbf{0}$, $P = 20$ dBm and HS-OFDM are considered for case #1 and case #2.
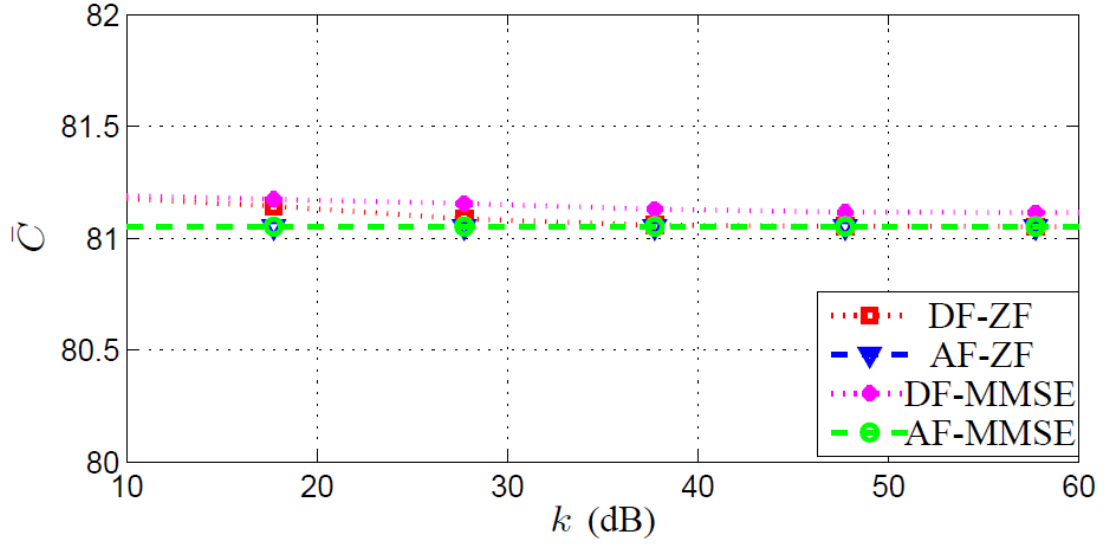
(a) case #3
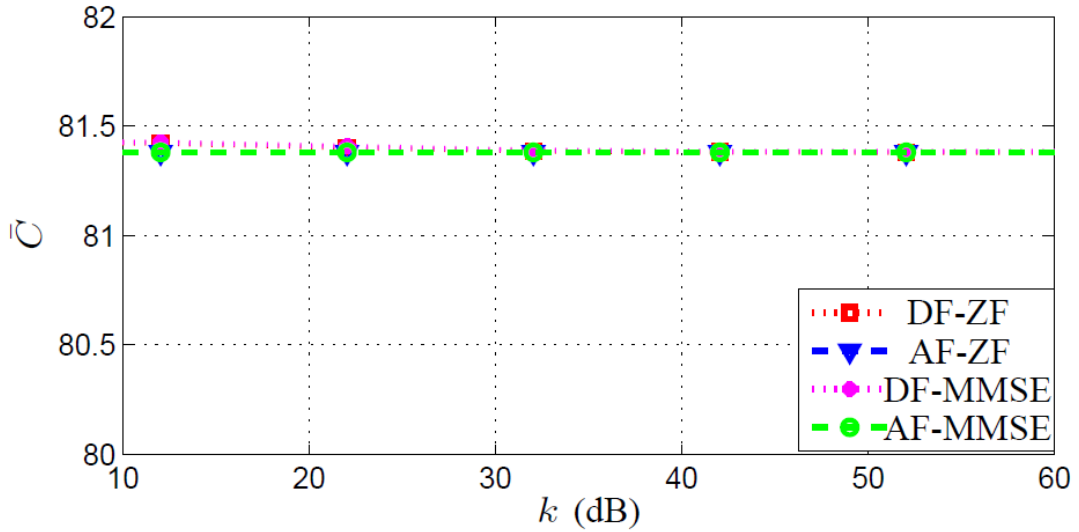
(b) case #4

Figure 23: Maximum data rates when $\mathbf{E} \neq \mathbf{0}$, $P = 20$ dBm and HS-OFDM are considered for case #3 and case #4.

6 CONCLUSIONS

This dissertation presented several analyses based on the data set obtained from a measurement campaign of cooperative and in-home PLC channels by considering a single relay model and the frequency bands 1.7-30 MHz, 1.7-50 MHz and 1.7-100 MHz. As the relay was located in different positions, it was possible to identify the scenarios and conditions under which cooperation is advantageous. In this regard, a comparison between theoretical channel capacities and maximum data rates (HS-OFDM scheme) of the relaying channel related to direct channel was discussed in detail. Besides, the performances of optimal and uniform power allocation were compared. While the first one requires the CSI of channel to optimally allocated the resource, the second adopts the same power for all subcarriers and disregards or ignores the use of such information.

Regarding the power allocation in all subcarriers, OA and UA have shown almost the same performance, although OA presented the best results, mainly if the transmission power decreases (efficient power allocation becomes more relevant when the channel conditions are difficult for data communications).

Considering the optimal allocated total power, we have established that the MRC technique presents the best performance and the EGC, the worst one on in-home and cooperative PLC channels. Furthermore, the HS-OFDM scheme together with FDE-MMSE attains performance similar to that of FDE-ZF. With respect to protocols, the AF protocol is not beneficial for low values of transmission power. The DF protocol presents gains in scenarios where the relay node is approximately at the midpoint between the S and D nodes and also when it is near to the S node or the D node, mainly for low values of transmission power. The 1.7-100 MHz frequency band offers the best results for the DF protocol while the 1.7-30 MHz frequency band attains the best results for the AF protocol.

The DF protocol ceases being advantageous in relation to the AF protocol as the symbol error probability at the relay node and/or the transmission power increases considerably. This result depends on what FDE technique is employed. For the MMSE, the DF protocol advantage is higher than that obtained for ZF.

For the uniformly allocated power, we can conclude that the MRC technique is more advantageous and HS-OFDM scheme together with FDE-MMSE attains almost the same performance as the FDE-ZF. Additionally, the AF protocol is beneficial for high values of transmission power, mainly for the 1.7-30 MHz frequency band. The DF protocol offers the highest gains only when low values of transmission power and the cases #1, #2 and #3 are considered, mainly for the 1.7-100 MHz frequency band.

Summarizing, based on a measured data set, it work described the conditions and scenarios under which the cooperative PLC system may be of interest for application in in-home electric power grids.

6.1   Future Works

Below, it is a list of topics to be examined in the future. The idea of them arose in the course of this dissertation.

1. To expand this measurement campaign to increase the number of residences.

2. To compare the performance of the HS-OFDM scheme with other data transmission schemes.

3. To consider multiple relays.

4. To take into account multihop scenario.

5. To evaluate the outage probability.

REFERENCES

[1] T. R. Oliveira, "The characterization of hybrid PLC-wireless and PLC channels in the frequency band between 1.7 and 100 mhz for data communication," Doctorate Thesis, Federal University of Juiz de Fora, Mar. 2015.

[2] F. J. Canete, J. A. Cortes, L. Diez, and J. T. Entrambasaguas, "Modeling and evaluation of the indoor power line transmission medium," *IEEE Communications Magazine*, vol. 41, no. 4, pp. 41–47, Apr. 2003.

[3] H. Hrasnica, A. Haidine, and R. Lehnert, *Broadband Powerline Communications: Network Design*, ser. NY.   John Wiley & Sons, 2005.

[4] M. Dohler and Y. Li, *Cooperative Communications: Hardware, Channel and PHY*. Cambridge: Wiley, 2010.

[5] G. Bumiller, L. Lampe, and H. Hrasnica, "Power line communication networks for large-scale control and automation systems," *IEEE Communications Magazine*, vol. 48, no. 4, pp. 106–113, Apr. 2010.

[6] Y. P. Hong, W. Huang, and C. J. Kuo, *Cooperative Communications and Networking*. New York: Springer, 2010.

[7] M. V. Ribeiro, G. R. Colen, F. V. P. Campos, Z. Quan, and H. V. Poor, "Clustered-orthogonal frequency-division multiplexing for power line communication: When can it be beneficial?" *IET Communications*, vol. 8, no. 13, pp. 2336–2347, Sep. 2014.

[8] K. Dostert, *Power Line Communications*, ser. NY.   Prentice Hall, 2001.

[9] H. C. Ferreira, L. Lampe, J. Newbury, and T. G. Swart, *Power Line Communications: Theory and Applications for Narrowband and Broadband Communications over Power Lines.*   John Wiley & Sons, 2010.

[10] G. Jee, C. Edison, R. Das Rao, and Y. Cern, "Demonstration of the technical viability of PLC systems on medium- and low-voltage lines in the united states," *IEEE Communications Magazine*, vol. 41, no. 5, pp. 108–112, May 2003.

[11] S. Galli, A. Scaglione, and Z. Wang, "For the grid and through the grid: The role of power line communications in the smart grid," *Proceedings of the IEEE*, vol. 99, no. 6, pp. 998–1027, Jun. 2011.

[12] S. Goldfisher and S. Tanabe, "IEEE 1901 access system: An overview of its uniqueness and motivation," *IEEE Communications Magazine*, vol. 48, no. 10, pp. 150–157, Oct. 2010.

[13] S. Galli and O. Logvinov, "Recent developments in the standardization of power line communications within the IEEE," *IEEE Communications Magazine*, vol. 46, no. 7, pp. 64–71, Jul. 2008.

[14] HD-PLC. New products. [Online]. Available: http://www.hd-plc.org/modules/products/index.html-acessedinSeptember2014.

[15] J. Egan. PLC neighboring networks. [Online]. Available: http://www.marvell.com/wireline-networking/ghn/assets/Neighboring-Networks.pdf-acessedinSeptember2014.

[16] Qualcomm. Powerline - performance is in the house. [Online]. Available: http://www.qca.qualcomm.com/networking/connected-home/powerline/-acessedinSeptember2014.

[17] M. Yigit, V. C. Gungor, G. Tuna, M. Rangoussi, and E. Fadel, "Power line communication technologies for smart grid applications: a review of advances and challenges," *Computer Networks*, vol. 70, pp. 366–383, Sep. 2014.

[18] F. J. Canete, J. A. Cortes, L. Diez, and J. T. Entrambasaguas, "A channel model proposal for indoor power line communications," *IEEE Communications Magazine*, vol. 49, no. 12, pp. 166–174, Dec. 2011.

[19] S. Galli and T. C. Banwell, "A deterministic frequency-domain model for the indoor power line transfer function," *IEEE Journal on Selected Areas in Communications*, vol. 24, no. 7, pp. 1304–1316, Jul. 2006.

[20] L. Lampe, R. Schober, and S. Yiu, "Distributed space-time coding for multihop transmission in power line communication networks," *IEEE Journal on Selected Areas in Communications*, vol. 24, no. 7, pp. 1389–1400, Jul. 2006.

[21] M. Biagi, "MIMO self-interference mitigation effects on power line relay networks," *IEEE Communications Letters*, vol. 15, no. 8, pp. 866–868, Aug. 2011.

[22] S. D'Alessandro, A. M. Tonello, and F. Versolatto, "Power savings with opportunistic decode and forward over in-home PLC networks," in *Proc. IEEE International Symposium on Power Line Communications and Its Applications*, Apr. 2011, pp. 176–181.

[23] S. D'Alessandro and A. M. Tonello, "On rate improvements and power saving with opportunistic relaying in home power line networks." *EURASIPJournal on Advances in Signal Processing*, vol. 2012, p. 194, 2012.

[24] L. Lampe and A. J. H. Vinck, "On cooperative coding for narrow band PLC networks," *International Journal of Electronics and Communications*, vol. 65, no. 8, pp. 681–687, Aug. 2011.

[25] K. Kim, H. Lee, Y. Kim, J. Lee, and S. Kim, "Cooperative multihop AF relay protocol for medium-voltage power-line-access network," *IEEE Trans. on Power Delivery*, vol. 27, no. 1, pp. 195–204, Jan. 2012.

[26] X. Cheng, R. Cao, and L. Yang, "Relay-aided amplify-and-forward powerline communications," *IEEE Trans. on Smart Grid*, vol. 4, no. 1, pp. 265–272, Mar. 2013.

[27] M. Noori and L. Lampe, "Improving data rate in relay-aided power line communications using network coding," in *Proc. IEEE Global Communications Conference*, Dec. 2013, pp. 2975–2980.

[28] Y. Kim, S. Choi, S. Kim, and J. Lee, "Capacity of OFDM two-hop relaying systems for medium-voltage power-line access networks," *IEEE Trans. on Power Delivery*, vol. 27, no. 2, pp. 886–894, Apr. 2012.

[29] K. J. R. Liu, A. K. Sadek, W. Su, and A. Kwasinski, *Cooperative Communications and Networking.* Cambridge: University Press, 2009.

[30] J. Anatory and N. Theethayi, *Broadband Power-line Communication Systems: Theory and Applications.* Boston: WIT Press, 2010.

[31] C. Choudhuri and U. Mitra, "Capacity bounds for relay channels with intersymbol interference and colored gaussian noise," *IEEE Trans. on Information Theory*, vol. 60, no. 9, pp. 5639–5652, Sep. 2014.

[32] K. U. Choi, C., Y. Kim, and G. Im, "Spectral efficient cooperative diversity technique with multi-layered modulation," *IEEE Trans. on Communications*, vol. 58, no. 12, pp. 3480–3490, Dec. 2010.

[33] G. R. Colen, C. A. G. Marques, T. R. Oliveira, F. P. V. de Campos, and M. V. Ribeiro, "Measurement setup for characterizing low-voltage and outdoor electric distribution grids for PLC systems," in *Proc. Conference On Innovative Smart Grid Technologies Latin America*, Apr. 2013, pp. 1–5.

[34] T. R. Oliveira, C. A. G. Marques, W. A. Finamore, S. L. Netto, and M. V. Ribeiro, "A methodology for estimating frequency responses of electric power grids," *Journal of Control, Automation and Electrical Systems*, vol. 25, pp. 720–731, 2014.

Appendix A – Publications

The list of publications during the master period are as follows:

- Michelle S. P. Facina and Moisés V. Ribeiro "The influence of the symbol detection error on cooperative in-home power line communication based on HS-OFDM scheme", *Simpósio Brasileiro de Telecomunicações*, 2015. (submitted)

- Michelle S. P. Facina, Haniph A. Latchman, H. Vincent Poor and Moisés V. Ribeiro; "Cooperative in-home power line communication: analyses based on a measurement campaign", *IEEE Transactions on Communication*, 2015. (submitted)

- Roberto O. Massi, Michelle S. P. Facina ; Alex B. Vieira, Moisés V. Ribeiro, "Um protocolo MAC de cooperação para redes PLC", in *XXXIII Simpósio Brasileiro de Redes de Computadores e Sistemas Distribuídos*, 2015, to be published.

- Michelle S. P. Facina and Moisés V. Ribeiro "The influence of transmission power and frequency bandwidth on in-home cooperative power line communication", *IEEE International Symposium on Power Line Communications and Its Applications*, 2015, to be published.

- Guilherme R. Colen, Michelle S. Pereira, Thiago R. Oliveira, Fabrício P. V. Campos, Moisés V. Ribeiro,"Setup de medição para caracterização de redes de distribuição de energia elétrica externas para sistemas PLC", *Seminário Nacional de Distribuição de Energia Elétrica*, 2014.

- Thiago R. Oliveira, Cristiano A. G. Marques, Michelle S. Pereira, Sérgio L. Netto, Moisés V. Ribeiro "The characterization of hybrid PLC wireless channels: a preliminary analysis", *IEEE International Symposium on Power Line Communications and Its Applications*, 2013.

- Thiago R. Oliveira, Fernando J. A. Andrade , Luis Guilherme, Michelle S. Pereira, Moisés V. Ribeiro,"Measurement of hybrid PLC-wireless channels for indoor and broadband data communication", *Simpósio Brasileiro de Telecomunicações*, 2013.

Appendix B – Electric Plants

B.1 Residence #1

This place comprises a house of 78 m^2, the disposal of power outlets can be seen in Figure 24.
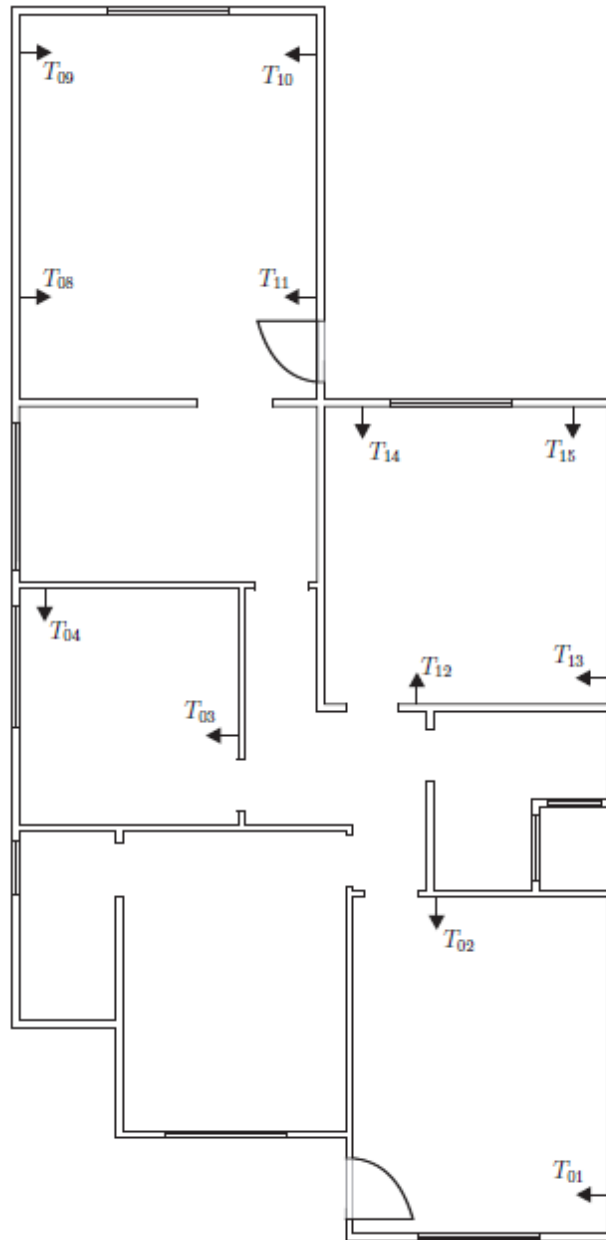
Figure 24: Layout of residence #1.

B.2 Residence #2

This place is a house of 69 m^2. The power outlets considered are shown in Figure 25.
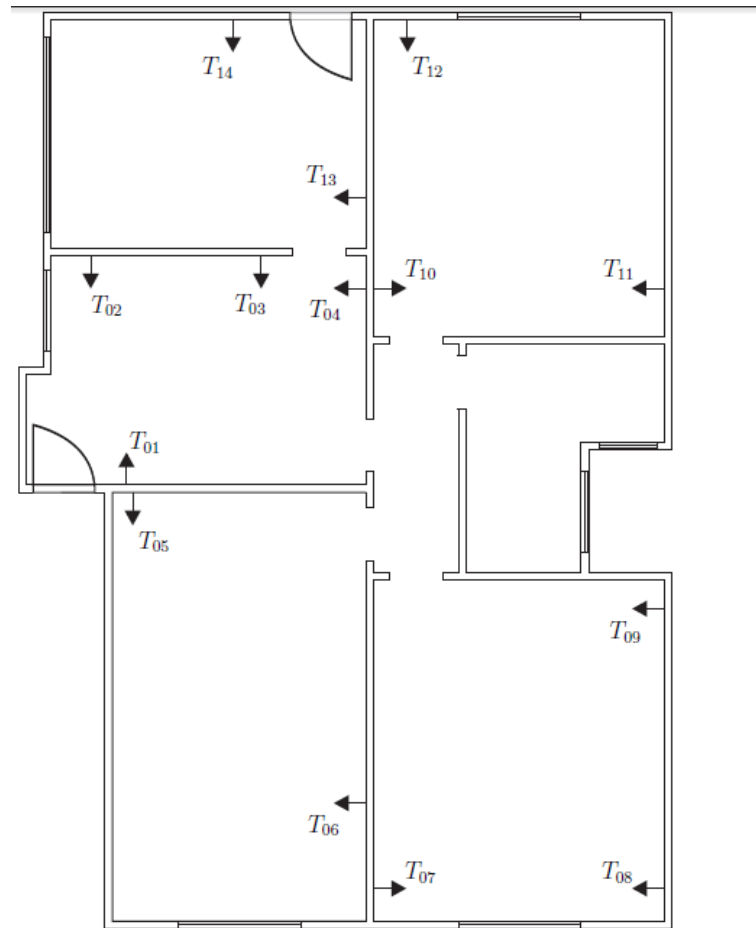
Figure 25: Layout of residence #2.

B.3 Residence #3

This place is an apartment of 54 m^2. The power outlets considered are shown in Figure 26.
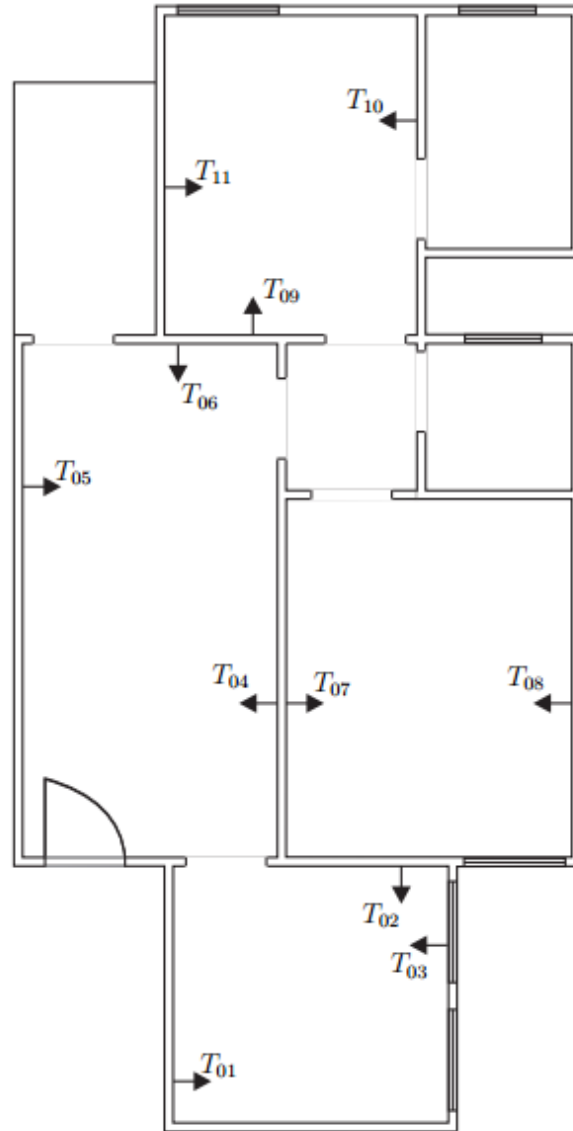
Figure 26: Layout of residence #3.

B.4   Residence #4

This place is an apartment of 42 m^2. The power outlets considered are shown in Figure 27.
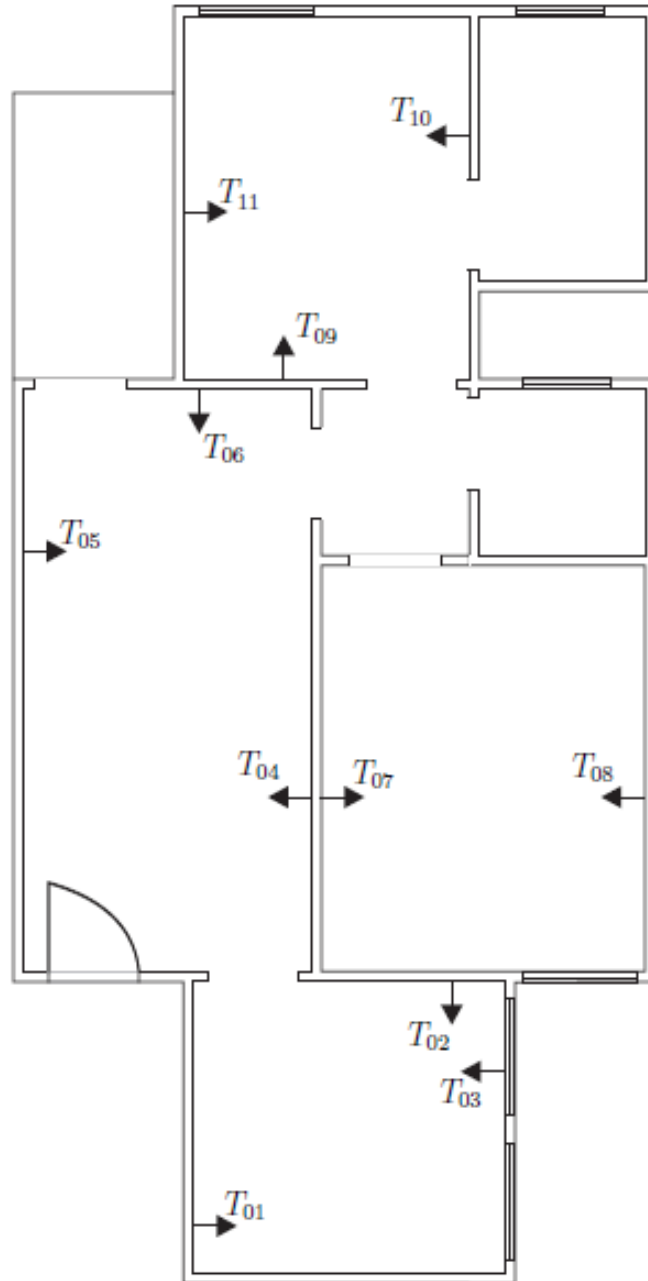
Figure 27: Layout of residence #4.

B.5   Residence #5

This place is an apartment of 65 m². The power outlets considered are shown in Figure 28.
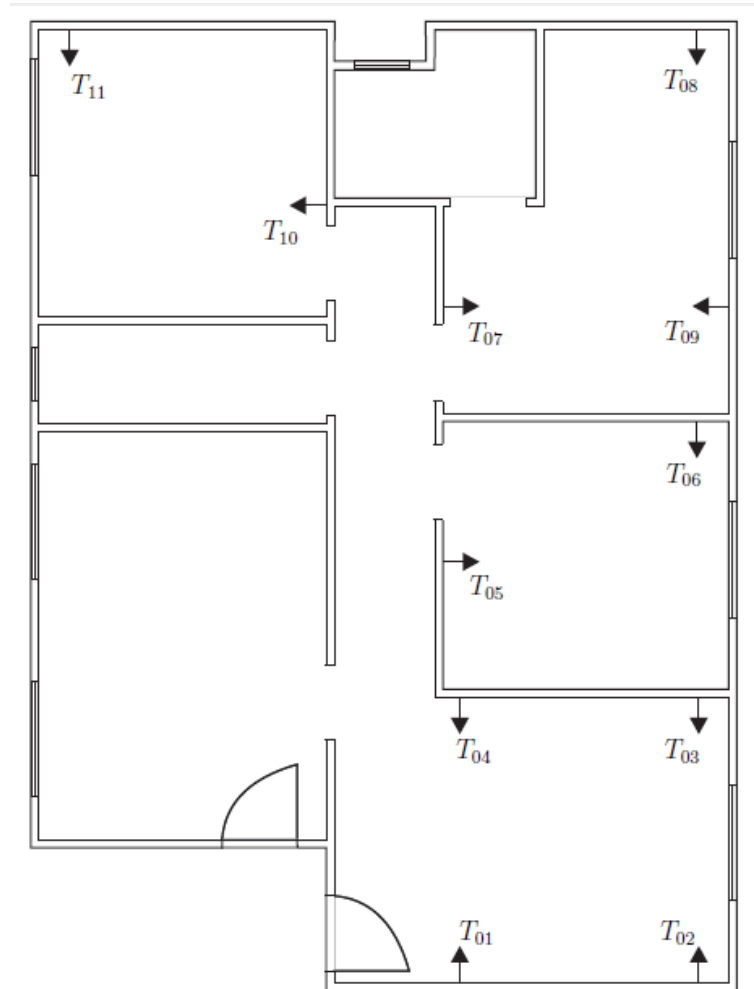
Figure 28: Layout of residence #5.

B.6 Residence #6

This place is an apartment of 62 m^2. The power outlets considered are shown in Figure 29.
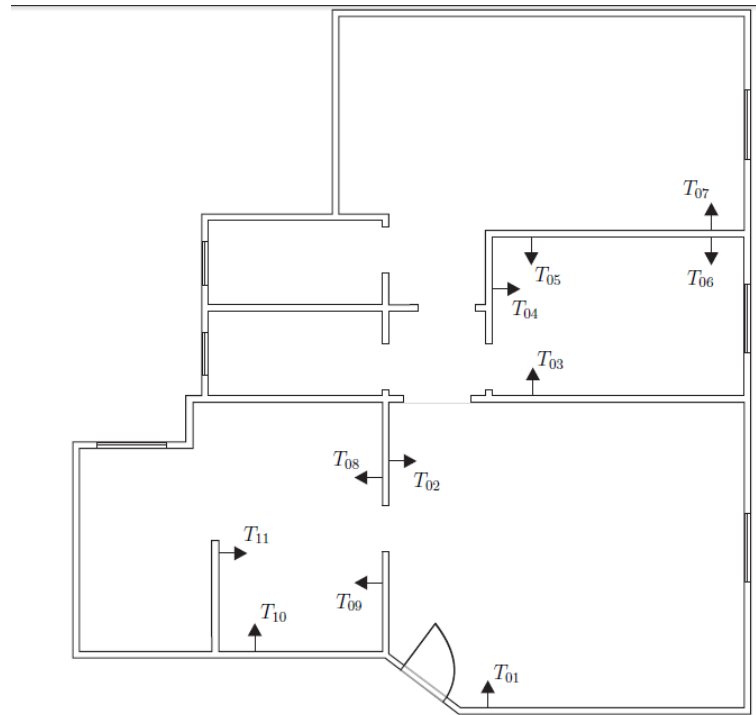
Figure 29: Layout of residence #6.

B.7 Residence #7

This place is an apartment of 54 m^2. The power outlets considered are shown in Figure 30.
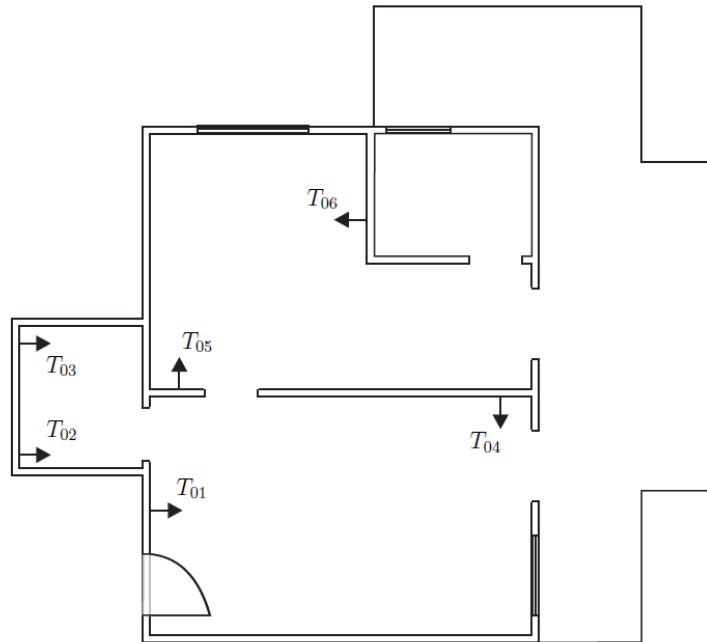
Figure 30: Layout of residence #7.